Journal of Medicinal Chemistry Article

J. Med. Chem. **2010,** *53,* 1159–1171 **1159**
DOI: 10.1021/jm9014636

Structure−Function Relationships and Crystal Structures of the Vitamin D Receptor Bound 2α-Methyl-(20*S*,23*S*)- and 2α-Methyl-(20*S*,23*R*)-epoxymethano-1α,25-dihydroxyvitamin D_3†

Pierre Antony,‡ Rita Sigüeiro,§ Tiphaine Huet,‡ Yoshiteru Sato,‡ Nick Ramalanjaona,‡ Luis Cezar Rodrigues,§ Antonio Mouriño,§ Dino Moras,*,‡ and Natacha Rochel*,‡

‡*Département de Biologie et de Génomique Structurales, Centre National de la Recherche Scientifique, Institut National de la Santé de la Recherche Médicale, Université de Strasbourg, CEBGS-IGBMC (Centre Européen de Biologie et Génomique Structurale—Institut de Génétique et de Biologie Moléculaire et Cellulaire), 1 Rue Laurent Fries, 67404 Illkirch, France and* §*Departamento de Química Orgánica and Unidad Asociada al CSIC, Universidad de Santiago de Compostela, 15782, Spain*

Received October 3, 2009

The vitamin D nuclear receptor is a ligand-dependent transcription factor that controls multiple biological responses such as cell proliferation, immune responses, and bone mineralization. Numerous 1α,25$(OH)_2D_3$ analogues, which exhibit low calcemic side effects and/or antitumoral properties, have been synthesized. We recently showed that the synthetic analogue (20*S*,23*S*)-epoxymethano-1α,25-dihydroxyvitamin D_3 (**2a**) acts as a 1α,25$(OH)_2D_3$ superagonist and exhibits both antiproliferative and prodifferentiating properties in vitro. Using this information and on the basis of the crystal structures of human VDR ligand binding domain (hVDR LBD) bound to 1α,25$(OH)_2D_3$, 2α-methyl-1α,25$(OH)_2D_3$, or **2a**, we designed a novel analogue, 2α-methyl-(20*S*,23*S*)-epoxymethano-1α,25-dihydroxyvitamin D_3 (**4a**), in order to increase its transactivation potency. Here, we solved the crystal structures of the hVDR LBD in complex with the **4a** (C23*S*) and its epimer **4b** (C23*R*) and determined their correlation with specific biological outcomes.

Introduction

The pleiotropic actions of the hormonally active metabolite of vitamin D_3, the seco-steroid 1α,25-dihydroxyvitamin D_3 (**1**, 1α,25$(OH)_2D_3$, Figure 1), are mediated through its binding to the cognate nuclear vitamin D receptor (VDR[a]), a ligand-dependent transcriptional modulator that belongs to the superfamily of steroid/thyroid hormone/retinoid nuclear receptors (NR).[1−3] Among the structural multidomains of NR, the ligand binding domain (LBD), located at the carboxy terminus, is a key transcriptional regulator because it harbors the ligand induced transactivation function 2 (AF-2).[4] Upon ligand complexation, the LBD undergoes a major conformational change involving the folding back of H12 onto the core of LBD, termed the "mouse-trap" mechanism.[5,6]

Activated VDR controls multiple long-term biological responses including cell growth, apoptosis, angiogenesis, antiproliferation, differentiation, bone mineralization, and calcium/phosphate homeostasis.[7−10] Therapeutic applications of pharmacological doses of 1α,25$(OH)_2D_3$, which encompass treatments for renal osteodystrophy, osteoporosis, psoriasis, cancer, autoimmune diseases, and prevention of graft rejection are limited because of the hormone's intrinsic hypercalcemic effect.[11] Therefore, the design of 1α,25$(OH)_2D_3$ analogues exhibiting antiproliferative and/or immunoregulatory properties with concomitant low calcemic side effect is the topic of intensive investigations at both mechanistic and clinical levels.[12−16] The development of such analogues has led to more than 3000 compounds with structural modifications on the A and/or CD rings or the aliphatic side chain. However, only a few of these are used to treat human diseases.[17,18]

In order to optimize the aliphatic side chain conformation with a subsequent entropy benefit, we recently designed and synthesized the 1α,25$(OH)_2D_3$ analogue, (20*S*,23*S*)-epoxymethano-1α,25-dihydroxyvitamin D_3 (AMCR277A, **2a**, C23*S*, Figure 1), which incorporates an oxolane ring in the side chain.[19] We showed that it acts as a 1α,25$(OH)_2D_3$ superagonist because it is able to mediate transcriptional activity with a magnitude at least 10-fold higher than that of the natural ligand. In addition, it has the capacity to inhibit the proliferation of the human promyelocytic HL60 cells and induce their differentiation into monocyte-like phenotype at concentrations much lower than 1α,25$(OH)_2D_3$. In contrast, we demonstrated that its epimer, (20*S*,23*R*)-epoxymethano-1α,25-dihydroxyvitamin D_3 (AMCR277B, **2b**, C23*R*, Figure 1), behaves like 1α,25$(OH)_2D_3$. Previous studies have shown that incorporation of an α-methyl at C2 of the A-ring of 1α,25$(OH)_2D_3$ does not result in superagonistic activity, although this compound (**3**, Figure 1) exhibits a 3-fold higher affinity to the VDR LBD relative to the natural ligand.[20,21] In order to improve the capacity of 1α,25$(OH)_2D_3$ agonists in stimulating transcription and cellular growth arrest, we undertook the structure-based design of novel 1α,25$(OH)_2D_3$

†The atomic coordinates and structure factors (PDB codes 3A3Z and 3A40) have been deposited in the Protein Data Bank, Research Collaboratory for Structural Bioinformatics, Rutgers University, New Brunswick, NJ (http://www.rcsb.org/).

*To whom correspondence should be addressed. For D.M.: phone, 33.3.88.65.32.20; fax, 33.3.88.65.32.76; e-mail, moras@igbmc.fr. For N.R.: phone, 33.3.88.65.57.81; fax, 33.3.88.65.32.76; e-mail: rochel@igbmc.fr.

[a]Abbreviations: NR, nuclear receptor; 1α,25$(OH)_2D_3$, 1α,25-dihydroxyvitamin D_3; LBD, ligand binding domain; VDR, vitamin D receptor; rmsd, root-mean-square deviation; (*S*)-p-tolBINAP, (*S*)-(−)-2,2′-bis(di-*p*-tolylphosphino)-1,1′-binaphthyl.

Published on Web 01/13/2010

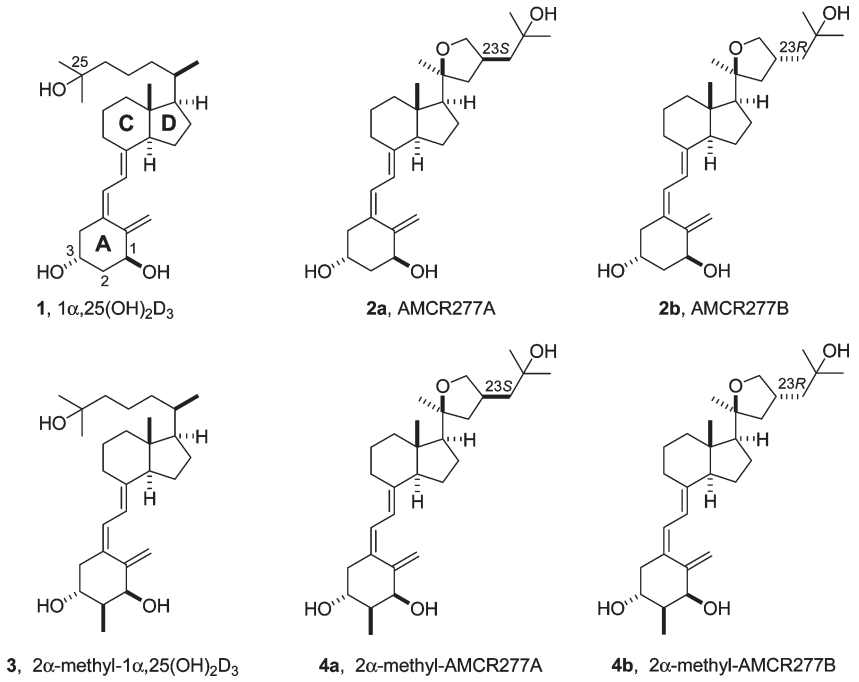

Figure 1. Chemical structures of the $1\alpha,25(OH)_2D_3$ and the analogues **2a**, **2b**, **4a**, and **4b**.

Scheme 1. Synthesis of Vitamin D_3 Analogues **2a** and **2b** by the Wittig−Horner Approach

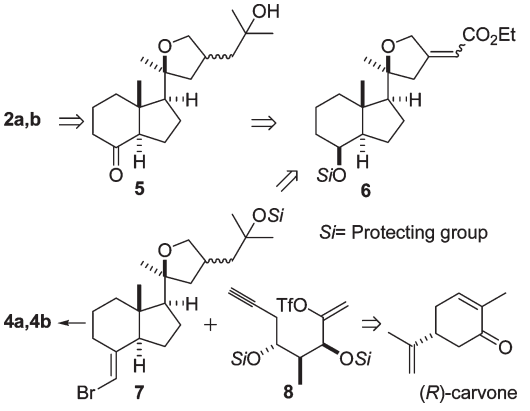

analogues, the (20*S*,23*S*)-epoxymethano-1α,25-dihydroxyvitamin D_3 (2α-methyl-AMCR277A, **4a**, C23*S*, Figure 1) and its epimer, the (20*S*,23*R*)-epoxymethano-1α,25-dihydroxyvitamin D_3 (2α-methyl-AMCR277B, **4b**, C23*R*, Figure 1). These new $1\alpha,25(OH)_2D_3$ analogues were synthesized to increase their stability in the ligand binding pocket (LBP) to enhance $1\alpha,25(OH)_2D_3$ superagonistic activity.

The present study aims at gaining insight into the structure−activity relationships of **4a**,**b**. To achieve this goal, we solved the crystal structures of the hVDR LBD bound to **4a** or to its epimer **4b** and highlight a sharp difference between the in vitro and the in vivo biological effects of the two $1\alpha,25(OH)_2D_3$ analogues.

Chemistry

We have recently described the synthesis of active $1\alpha,25(OH)_2D_3$ analogues **2a** and **2b** (Figure 1) by Lythgoe's Wittig−Horner approach using ketones **5** as the CD side chain building block. These ketones were prepared by catalytic hydrogenation of unsaturated esters **6** followed by the following sequence:

Scheme 2. Asymmetric Reduction of Unsaturated Esters **9a** and **9b**[a]

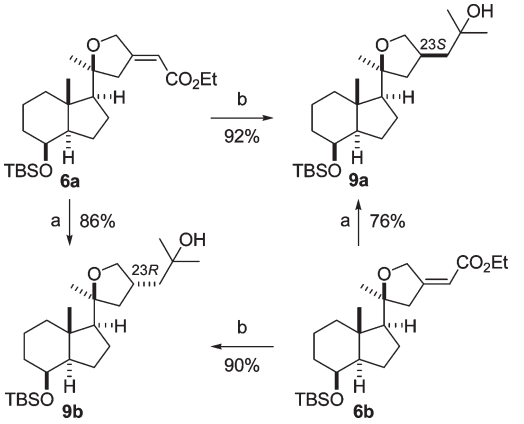

[a] Reagents and conditions: (a) PMHS, CuCl, KO*t*-Bu, (*S*)-tolBINAP, *i*-PrOH, hexanes, −25 °C, ultrasound, 1 h; then MeLi, THF, −78 °C → room temp; (b) same as in step a but with (*R*)-tolBINAP instead of (*S*)-tolBINAP.

methylation, separation of the resulting tertiary alcohols, desilylation, and oxidation (Scheme 1).[19] We now report the synthesis of $1\alpha,25(OH)_2D_3$ analogues **4a** and **4b** from (*R*)-carvone (A-ring precursor) and involving a stereoselective route to the CD-building block. The key features of the new synthetic strategy involve (1) palladium-catalyzed coupling between enoltriflate **8** and alkenylzinc intermediates derived from **7**, (2) stereoselective synthesis of bromides **7** from **6**, and (3) synthesis of enoltriflate **8** from (*R*)-carvone.

Synthesis of Alkenyl Bromides 7. Separation of a 1:1 mixture of (*E*,*Z*)-unsaturated esters **6**[19] by HPLC provided pure (*E*)-ester (**6a**, less polar compound) and (*Z*)-ester (**6b**, more polar compound) (Scheme 2). The stereochemistry of both isomers was established by NOE experiments (=C**H**CO_2Et). Asymmetric conjugate reduction of unsaturated ester **6a** under Buchwald conditions[22] employing catalytic

Scheme 3. Synthesis of the Upper Alkenyl Bromides **7a** and **7b**[a]

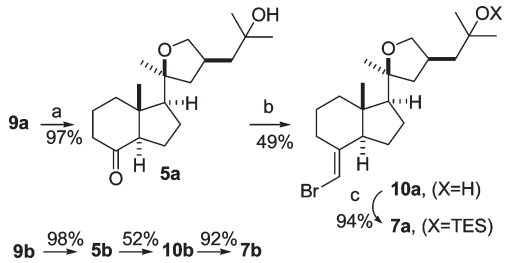

[a] Reagents and conditions: (a) TBAF, THF, reflux, 4 days; PDC, CH_2Cl_2, room temp, 12 h; (b) $(Ph_3PCH_2Br)Br$, NaHMDS, THF; (c) Et_3SiCl (TESCl), Im, DMAP, DMF, 0 °C → room temp, 12 h.

Scheme 4. Synthesis of the A-Ring Fragment[a]

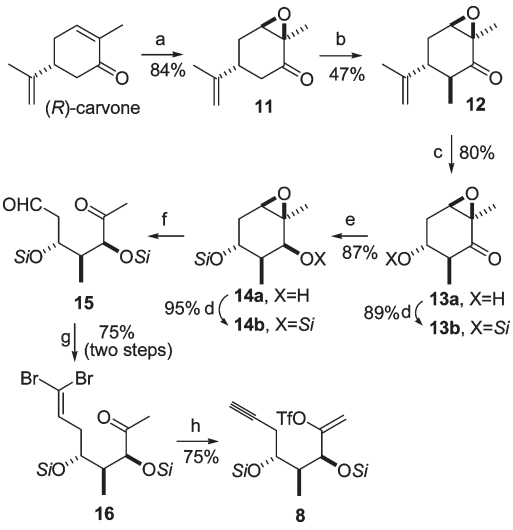

[a] Reagents and conditions: (a) H_2O_2, $LiOH \cdot H_2O$, MeOH, 0 °C, 30 min; (b) NaH, THF, room temp, 1 h; MeI, 0 °C, 5 h (47%); (c) O_3, $MeOH-CH_2Cl_2$, −78 °C; Ac_2O, Et_3N, DMAP, −35 °C → 78 °C, 2 h; NaOAc, MeOH, 37 °C, 12 h; (d) TBSCl (*t*-$BuMe_2SiCl$), imidazole, DMF, room temp, 12 h; (e) L-Selectride, THF, −78 °C, 30 min; (f) H_5IO_6, Et_2O, room temp, 12 h; (g) Ph_3P, Zn, CBr_4, CH_2Cl_2, 45 min; (h) LDA, THF, −78 °C, 1 h; *n*-BuLi, 15 min,; 5-Cl-py-2-NTf_2, −78 °C → room temp, 12 h.

(*R*)-p-tolBINAP/CuCl/KO*t*-Bu and poly(methylhydrosiloxane) (PMHS) as the reducing agent and *i*-PrOH as the proton source provided (C23*S*)-alcohol **9a**[19] in 92% yield. The use of the enantiomeric ligand (*S*)-p-tolBINAP gave (C23*R*)-alcohol **9b**[19] in 86% yield. This strategy allows the preparation of **9a** (precursor of superagonist **2a**) or **9b** as the only products from either unsaturated esters **6a** or **6b**. The above synthetic route allows the preparation of alcohol **9a** or **9b** in high yield from either ester **6a** or **6b**. The previous synthetic route[19] provides a mixture of alcohols **9a** and **9b**.

Alcohols **9a** and **9b** were converted to the corresponding ketones **5a** and **5b** as previously described.[19] Wittig olefination of **5a** and **5b** by the method of Trost[23] followed by silylation provided the required alkenyl bromides **7a** and **7b** in 46% and 48% yield, respectively (two steps) (Scheme 3).

Synthesis of A-Ring Fragment 8. The synthesis of enoltriflate **8**, precursor of the A-ring, started with (*R*)-carvone[24] (Scheme 4). Stereoselective epoxidation of (*R*)-carvone provided the known epoxide **11**[24g,25] in 84% yield. Treatment of **11** with sodium hydride and alkylation with methyl iodide gave the monoalkykated product **12** in 47% yield, together with the corresponding dialkylated compound (29%). The stereochemistry of the methylation product **12** can be explained by protonation of the corresponding enolate. Degradation of the isopropenyl side chain[25b] of **12** by ozonolysis and subsequent reaction of the resulting intermediates with acetic anhydride followed by treatment with sodium acetate provided the desired alcohol **13a** in 80% yield. Silylation of **13a** with *tert*-butyldimethylsilyl chloride followed by reduction of the resulting silylated compound **13b** with lithium selectride followed by protection afforded the disilylated epoxide **14b** (77% yield for the three steps). The sterochemical outcome of the reduction product **14a** can be explained by L-Selectride attack to ketone **13b** from the less hindered face. The structure of compound **14a** was established by NOE experiments (see Supporting Information). Periodic acid-oxidative cleavage of **14b** generated the aldehyde **15** which was transformed into the vinylic dibromide **16** by olefination with $Ph_3P{=}CBr_2$ (75% yield, 2 steps). Conversion of **16** to the desired enoltriflate **8** was carried out in 75% yield using conditions previously reported for the corresponding unalkylated compound:[24i] base treatment (LDA and *n*-BuLi) to form the triple bond and the enolate and trapping of the latter with *N*-(5-chloro-2-pyridyl)bis(trifluoromethanesulfonimide).

Scheme 5. Formation of the Triene System by Pd(0)-Catalyzed Tandem Cyclization Negishi Coupling[a]

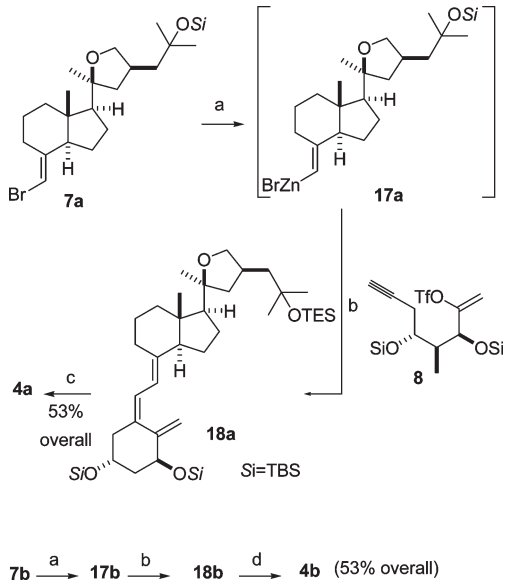

[a] Reagents and conditions: (a) *t*-BuLi, THF, −78 °C, 1 h; $ZnBr_2$, THF, −78 °C → 0 °C, 1 h; (b) **8**, $(Ph_3P)_4Pd$, Et_3N , THF, 12 h; (c) *n*-Bu4NF, THF, room temp, 24 h; (d) HF·Py, CH_2Cl_2, CH_3CN, Et_3N, room temp, 2 h.

Synthesis of the Target 1α,25(OH)$_2$D$_3$ Analogues 4a and 4b. For the construction of the vitamin D triene system, we chose the convergent Pd(0)-catalyzed tandem cyclization Negishi coupling approach recently developed in our laboratories.[24k] The alkenylzinc intermediate **17a** (CD side chain building block, Scheme 5) was prepared by metalation of alkenyl bromide **7a** with *t*-BuLi followed by transmetalation with $ZnBr_2$. Addition of the enoltriflate **8**, triethylamine, and catalytic tetrakis(triphenylphosphine)palladium(0) gave, after desilylation, the desired analogue **4a** in 55% yield. The other analogue **4b** was prepared in a similar way (53% yield) from alkenyl bromide **7b**.

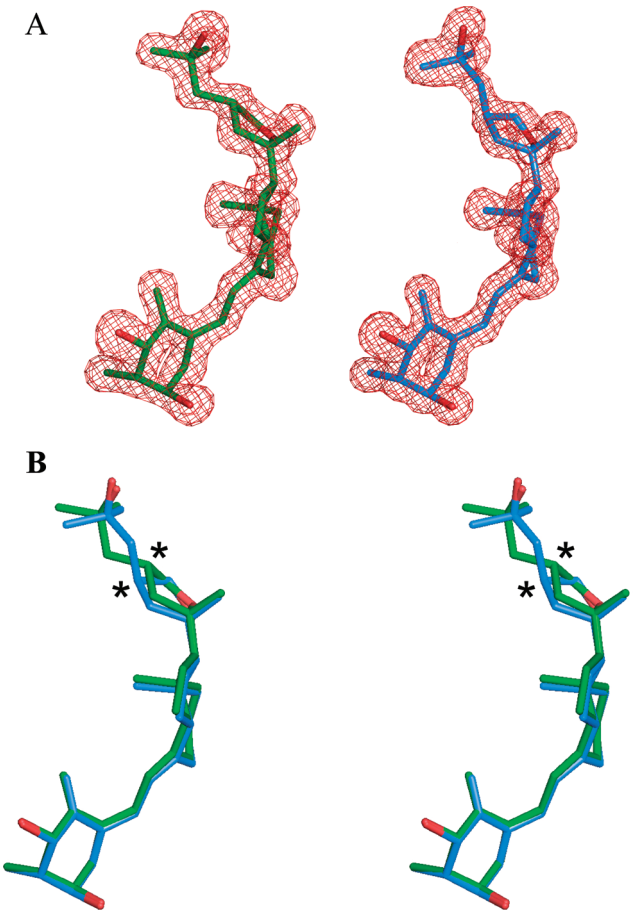

Figure 2. Conformation of the bound ligand. (A) The **4a** (left) and **4b** (right) are shown in the $F_o - F_c$ electron density omit map contoured at 3σ. The ligands are shown in stick representation with carbon atoms in green for **4a** and blue for **4b**, and oxygen atoms are in red. (B) A stereoview of the ligand conformations of **4a** (green) and **4b** (blue) in the VDR ligand binding pocket after superimposition showing the different side chain conformation of the two epimers. The chiral atoms at C23 are marked by asterisks.

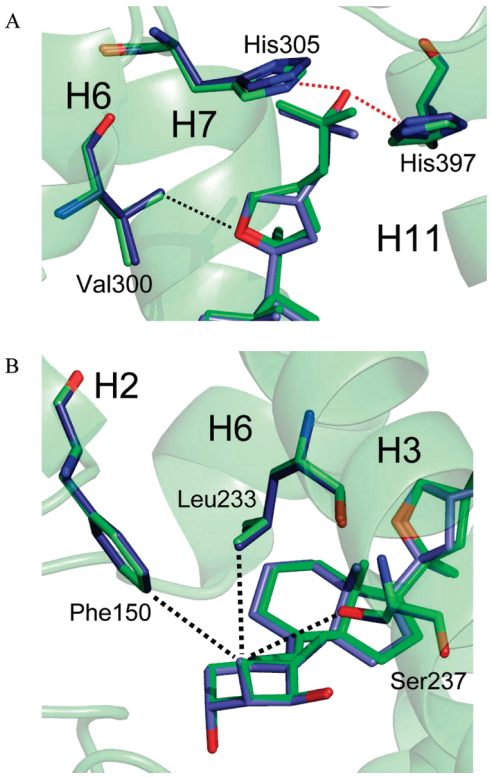

Figure 3. Detailed structural representation of both analogues bound to hVDR LBD around the aliphatic chain (A) and the 2α-methyl group (B) showing the characteristic residues involved in interactions. **4a** and **4b** are shown in green and blue, respectively. Oxygen and nitrogen atoms in VDR/**4a** and VDR/**4b** structures are shown in red and blue, respectively. Hydrogen and van der Waals bonds are shown in red and black dotted lines, respectively. Secondary structure of VDR is shown in cartoon. H2, H3, H6, H7, and H11 indicate helices.

Results

Overall Structures of the hVDR LBD Bound to 4a or 4b. The hVDR LBD mutant lacking 50 residues in the loop connecting helices H2 and H3 was used for the X-ray analyses of the hVDR LBD in complex with **4a** or **4b**. The same mutant was used to solve the structure of the hVDR LBD bound to 1α,25$(OH)_2D_3$ and to several 1α,25$(OH)_2D_3$ analogues, since the biological properties of this mutant such as ligand binding and transactivation in distinct cell lines are the same as those of the wild type.[6,26−28] Isomorphous crystals were obtained in similar conditions, and the crystal structures of hVDR LBD bound to **4a** or **4b** were determined at a resolution of 1.7 and 1.45 Å, respectively (Supporting Information Table 1).

Complexes of hVDR LBD with **4a** or **4b** adopt the canonical conformation of all previously reported agonist-bound nuclear receptor LBDs with 12 or 13 α-helices organized in a three-layered sandwich. In all the structures of hVDR LBD bound to agonist ligands, a unique conformation of the complex is observed. The position and conformation of the activation helix H12 are strictly maintained. The ligand adopts the same orientation in the pocket. An adaptation of their conformation is observed to maintain the hydrogen bonds forming the anchoring points. Compared to the structure of hVDR LBD in complex 1α,25$(OH)_2D_3$, the atomic coordinates of all Cα atoms of hVDR bound to **4a** and to **4b** show an rmsd of 0.18 and 0.15 Å, respectively. The ligand is buried in the predominantly hydrophobic pocket. The volumes of the ligands are 418, 416, and 396 $Å^3$ for **4a**, **4b**, and 1α,25$(OH)_2D_3$, respectively. The volume of the ligand binding cavity is 685, 682, and 673 $Å^3$ and the ligands occupy 61%, 61%, and 59% of the pocket for **4a**, **4b**, and 1α,25$(OH)_2D_3$, respectively.

Ligand−Protein Interactions. The A, seco-B, C, and D rings present conformations that are similar to those observed in the presence of the natural ligand (Figure 2). The distances between the 1-OH and the 25-OH groups are 12.9, 13.1, and 12.8 Å for hVDR LBD bound to **4a**, **4b**, and 1α,25$(OH)_2D_3$, respectively. The hydroxyl groups make the same hydrogen bonds as hVDR LBD bound to 1α,25-$(OH)_2D_3$ complex, 1-OH with Ser237 and Arg274, 3-OH with Tyr143 and Ser278, and 25-OH with His305 and His397.

A comparison of the aliphatic chain of **4a** to those of the previous nonmethylated **2a** and **2b**[19] reveals that the specific van der Waals interactions of the side chain with His-305, His-397, Val-418 and of the O21 atom of the oxolane ring with Val300 are conserved (Figure 3A). Similar to **2b**, the additional van der Waals contact of O21 with Val300 is weaker in the VDR−**4b** complex. This interaction with Val300 has been observed in some hVDR LBD crystal

structures with superagonist ligands 1α,25-dihydroxy-20-epi-22-oxa-24a,26a,27a-trihomovitamin D_3 (KH1060) or 19-nor-14-epi-23-yne-1,25-$(OH)_2D_3$ (TX522).[28,29] The stereoisomer **4b** presents an energetically unfavorable oxolane ring and adopts a different side chain conformation because of the inverse configuration at C23 which affects the positions of C25, C26, C27, and 25-OH and destabilizes the activation helix-12 (Val418) compared to **4a**.

The introduction of a methyl group at the 2α position does not modify the A-ring chair conformation of each ligand. The 2α-methyl group fills a small cavity of the pocket and makes additional van der Waals interactions with Phe150, Leu233, and Ser237 (Figure 3B), contacts also observed in the hVDR LBD complexed to 2α-methyl-1α,25$(OH)_2D_3$.[20] The previously reported crystal structures of hVDR LBD in complex with 1α,25$(OH)_2D_3$ and several synthetic ligands revealed the presence of tightly bound water molecules forming a channel near the C2 position of the ligand, which may play important roles in protein stability.[20] This water channel is also conserved in the two present **4a** and **4b** complexes, and the *B*-factors of the three waters (7.0, 6.4, and 3.3 $Å^2$ for the hVDR LBD/**4a** complex and 12.4, 11.9, and 10.3 $Å^2$ for the **4b** complex, respectively) are significantly lower than the average value of all water molecules (28.1 and 32.3 $Å^2$ for the hVDR LBD/**4a** complex and **4b** complex, respectively).

Table 1. Dissociation Constants of the SRC-1 Peptide to hVDR LBD in Response to 1α,25$(OH)_2D_3$ Analogues

analogues	relative dissociation constants
no ligand	no binding
1α,25$(OH)_2D_3$	1
2a	0.9 ± 0.2
2b	1.7 ± 0.2
4a	1.3 ± 0.2
4b	3.2 ± 0.2

Binding Affinity of the SRC-1 Peptide to hVDR LBD Bound to 2a or 4a Is Similar. To check the ligand effect on the recruitment of coactivator peptide to VDR, binding of fluorescently labeled SRC-1 peptide to hVDR LBD bound to 1α,25$(OH)_2D_3$, **2a**, **2b**, **4a**, and **4b** was monitored by fluorescence anisotropy. In its apo form, hVDR LBD does not bind the SRC-1 coactivator peptide. The magnitude of the SRC-1 binding when complexed to **2a** or **4a** was similar to that obtained with the natural ligand. In contrast, the **4b** ligand induces a 3-fold weaker binding between hVDR LBD and the SRC-1, whereas its parental analogue **2b** lowers it by 1.7-fold (Table 1). Therefore, stereochemistry of the C23 is a significant parameter for the recruitment of the SRC-1 peptide.

4a Is a More Potent 1α,25$(OH)_2D_3$ Superagonist Than 2a. Using gene reporter assays, we recently reported that **2a** shows superagonistic biological activities because it stimulates transcription 12-fold more than the natural ligand at 0.1 nM.[19] Methylation at the C2α position of the 1α,25-$(OH)_2D_3$ A ring induces a 3-fold increase of the binding affinity of hVDR LBD. Hence, we postulate that C2α methylation of **2a** may further increase its superagonist character.

Here, we demonstrate that at 0.1 nM, the transcription activity upon **4a** stimulation is 13- and 3.8-fold higher than those induced by the natural ligand and **2a**, respectively. Furthermore, at 5 nM **4a** achieves optimal VDR-directed transcription, whereas **4b** is 4 times less potent under similar stimulatory conditions in transactivation assays and behaves like the natural ligand (Figure 4). The dose-dependent comparison between **2a** and its new to 2α-methyl derivative reveals that at 0.1, 1, and 5 nM, the transcription activities induced by **2a** are only 26%, 42%, and 73% of that obtained

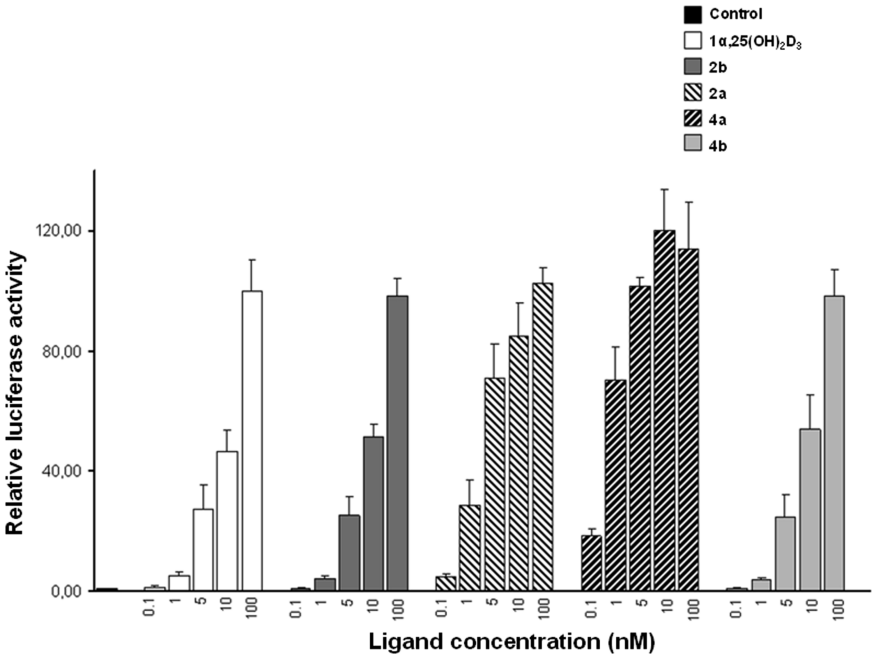

Figure 4. **4a** acts as an 1α,25$(OH)_2D_3$ superagonist in vitro. Transient transfections and luciferase reporter gene assays using MCF-7 human breast cancer cells were performed as reported in Experimental Procedures. Relative luciferase activities were calculated by dividing the luciferase activity by the respective β-galactosidase activity to correct for differences in transfection efficiency. For every triplicate the mean and the standard deviation were calculated. A two-tailed, paired Student's *t* test was performed when appropriate, and *p* values were calculated with reference to stimulation of hVDR with the solvent.

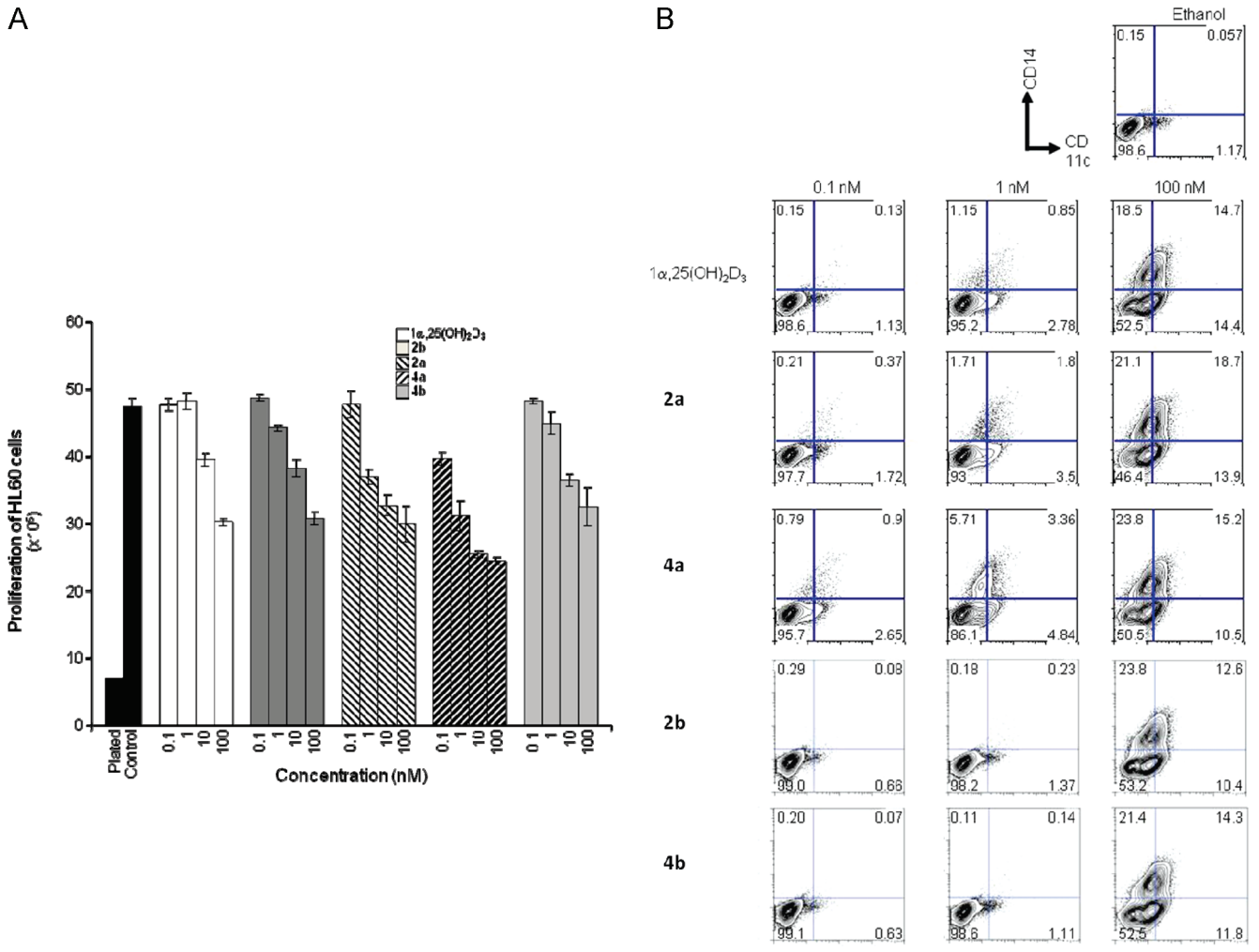

Figure 5. **4a** displays higher HL60 cell antiproliferation and prodifferentiating potency relative to its parental analogue **2a**. (A) **4a** mediated HL60 cell growth arrest is achieved for a dose of 0.1 nM. HL60 cells were incubated for 96 h with various concentrations of $1\alpha,25(OH)_2D_3$, **2a**, **2b**, **4a**, or **4b** versus control (ethanol 0.7%) and are counted. Data are presented as the mean ± SEM. (B) **4a** mediated HL60 differentiation into monocyte-like cells is achieved for a dose of 0.1 nM. Cells were labeled with PE-labeled antihuman CD11c and FITC-labeled antihuman CD14, and HL60 cell differentiation was estimated by the double-positive CD11c/CD14 subpopulation. Data are representative of three distinct experiments.

in the presence of **4a**, respectively. In summary, **4a** is a more potent superagonist compared to **2a** while its epimer **4b** is as active as the natural ligand (**1**).

Only 4a at 0.1 nM Induces HL60 Cell Proliferation Arrest with Concomitant Differentiation. Our previous data showed that the superagonistic property of **2a** is associated with a higher ability, compared to the natural ligand, to inhibit the proliferation of HL60 promyelocytic cell and to trigger their subsequent differentiation into monocyte-like phenotype as evidenced by the up-regulation of cell surface markers CD11c and CD14.[19] We further examined the effects of **4a** and **4b** in directing HL60 cell fate. Here, we found that the dose-dependent profile of **4b** in mediating HL60 cell arrest and differentiation is similar to that induced by **2b**. In sharp contrast, a dose of only 0.1 nM of **4a** is able to significantly reduce HL60 cell proliferation, whereas no effect at this concentration was observed for the other $1\alpha,25(OH)_2D_3$ analogues, including its parental analogue **2a**, compared to control incubations (Figure 5A). A similar proliferation pattern was detected when HL60 cells were incubated with 1 nM $1\alpha,25(OH)_2D_3$ agonists. Consistent with cell proliferation data, a 10-fold gain in the induction of HL60 cells differentiation was obtained with 0.1 nM **4a**, as a new double positive CD11c/CD14 subpopulation was detected compared to the other $1\alpha,25(OH)_2D_3$ analogues (Figure 5B). Moreover, single positive CD11c and CD14 cell populations were more abundant relative to **2a** and the natural ligand (at least 1.5- and 3-fold increase, respectively). A similar profile was observed with 10 nM $1\alpha,25(OH)_2D_3$ analogues treatment, and a lower or equal dose of 2α-methyl-$1\alpha,25(OH)_2D_3$ achieves neither antiproliferation nor differentiation of HL60 cells (data not shown). Therefore, C2α methylation of **2a** increases its ability to inhibit HL60 cell proliferation with concomitant differentiation into monocyte-like phenotype.

At low dose, 4a is more calcemic than $1\alpha,25(OH)_2D_3$. Whereas 4b Displayed in Vivo Low Calcemic Action Compared to the Natural Ligand. Using C57BL/6J mice, we previously showed that **2a** exhibits higher calcemic action than $1\alpha,25(OH)_2D_3$, whereas **2b** has an in vivo low calcemic effect than the natural ligand.[19] We monitored the calcium serum level of male mice that were subjected to 0.1 μg/kg intraperitoneal injections (ip) of $1\alpha,25(OH)_2D_3$ analogues versus untreated (control) ones. Mice survive during the

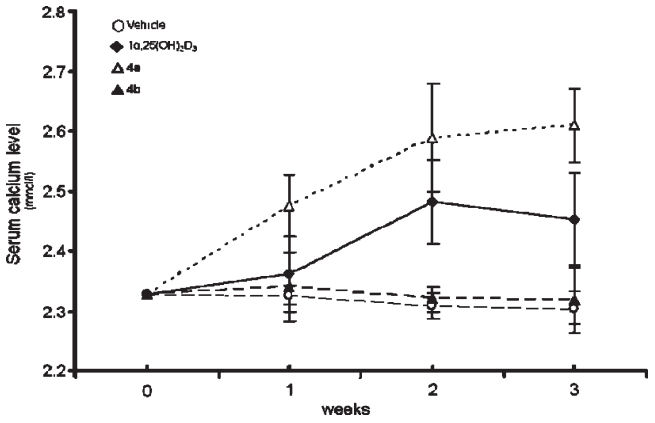

Figure 6. **4a** is more calcemic than **2a** or 1α,25(OH)$_2$D$_3$, whereas **4b** is less calcemic. Mice (6 weeks old; 6−7 mice/group) were injected intraperitoneally with 1α,25(OH)$_2$D$_3$, **4a**, **4b**, or sesame oil (vehicle) for 3 weeks. A single dose of 0.1 μg/kg was administrated every second day, and calcium serum level was weekly monitored: (open diamond) control, (black diamond) 1α,25(OH)$_2$D$_3$, (open triangle) **4a**, and (black triangle) **4b** incubations. Data are presented as the mean ± SEM.

3 weeks of the experiments, and their physiological state was satisfactory in response to the different analogues (data not shown). We observed that mice treated with **4b** leads to calcemic values that are similar to those induced by sesame oil as vehicle incubations. In contrast, ip injections of **4a** promote a robust calcium increase in the serum of mice, which is even higher than that detected with the natural ligand and similar to **2a**[19] (Figure 6). Thus, C2α methylation of **2a** improves the superagonist character of its parental analogue but not its calcemic property.

Discussion

The present study reports the crystal structures of the human VDR LBD bound to novel 1α,25(OH)$_2$D$_3$ analogues, the **4a**, and its epimer **4b** and describes their in vitro and in vivo biological effects. The rationale to undertake this study was based on three distinct observations: (i) compared to the crystal structure of hVDR LBD in complex with its natural ligand, those with 2α-methyl-1α,25(OH)$_2$D$_3$ and **2a** show different van der Waals interactions that may explain in part their biological action; (ii) 2α-methyl-1α,25(OH)$_2$D$_3$ displays higher binding affinity for hVDR LBD compared to 1α,25-(OH)$_2$D$_3$; (iii) **2a** is a 1α,25(OH)$_2$D$_3$ superagonist or has the capacity to better induce the differentiation of HL60 cells into monocyte-like phenotype than the natural ligand, while its epimer behaves like the natural ligand.[19,20] Thus, a methylation at the C2α of the A ring combined with an incorporation of an oxolane ring in the side chain leads to a new 1α,25-(OH)$_2$D$_3$ analogue that may behave as a more potent superagonist associated with stronger antitumoral properties in vitro. Therefore, we synthesized the **4a** and its epimer **4b** (Figure 1) and investigated their structure−function relationships.

Atomic resolution of the crystal structure of the hVDR LBD bound to **4a** reveals that this complex inherits structural features of both 2α-methyl-1α,25(OH)$_2$D$_3$ and **2a**, as evidenced by the specific van der Waals contacts of the 2α-methyl group with Phe150, Leu233, Ser237 and of the O21 atom of the oxolane ring with Val300 (Figure 3). As previously reported for hVDR LBD bound to agonist ligands, helix 12 adopts the canonical orientation, sealing the ligand binding cavity.[22,30,31] Comparison of complexes formed by hVDR LBD with **2a**, 1α,25(OH)$_2$D$_3$ or 2α-methyl-1α,25(OH)$_2$D$_3$, indicates that the new ligand **4a** displays an increased number of van der Waals contacts with the LBP than the other ones. These additional contacts may explain in part the higher potency of **4a** in mediating VDR-dependent transcription. Although 2α-methyl-1α,25(OH)$_2$D$_3$ displays a higher binding affinity for hVDR LBD relative to its natural ligand, it does not exhibit superagonist properties. On the other hand, we have shown that **2a** displays superagonistic biological activities.[19] Therefore, methylation at the C2α of the **2a** analogue synergistically increases its superagonistic character (Figure 4). In contrast, C2α methylation of **2b** does not improve its ability to further induce VDR-directed transcription compared to its parental **2b** analogue or the natural ligand (Figures 2 and 3). Because of the inverse configuration at C23, the stereoisomers **4b** and **2b** adopt a different side chain conformation compared to **4a** and **2a** affecting their respective contacts with activation helix 12 and resulting in a weaker activation. This property is conserved in the **4b** relative to **4a**, demonstrating that the active form of the bound ligand favored by the ring pucker is an essential parameter that directs the magnitude of VDR-induced transcription and HL60 cell antiproliferation/prodifferentiation (Figures 4 and 5).

Previous studies have shown that stronger VDR−coactivator interactions underlie the superagonistic activity of 1α,25(OH)$_2$D$_3$ analogues, such as 14-epi analogues.[28] To gain insights into the potential molecular mechanisms that may explain the superagonistic strength of **4a** relative to **2a**, we determined the binding affinity of the coactivator SRC-1 peptide to hVDR LBD incubated with each analogue. A higher recruitment of SRC-1 to hVDR LBD upon binding to **4a** does not account for its increased superagonist character, as **4a** induces weaker binding between hVDR LBD and the SRC-1 peptide compared to either 1α,25(OH)$_2$D$_3$ or **2a** which induces a binding efficiency fully comparable to that obtained with the natural ligand (Table 1). Therefore, larger domains of SRC-1 or other coactivators may play a key role in VDR-dependent transcription in response to **4a**.

Since the **2a** superagonist character is associated with a more potent ability to inhibit HL60 cell proliferation with concomitant differentiation into monocyte-like cells, we postulate that increased stabilization of the complex hVDR LBD bound to **4a** would result in a higher capacity to reduce HL60 cell growth arrest at low concentrations. We recapitulated the profile of each previously described 1α,25(OH)$_2$D$_3$ analogue in the modulating HL60 cell fate, namely, **2a** at 1 nM induces HL60 cell antiproliferation, whereas **2b** behaves like the natural ligand.[19] We now show that **4a** induces a 10-fold gain in lowering HL60 cell proliferation, as 0.1 nM **4a** leads to a significant decrease of HL60 cells number, whereas no effect was observed at this concentration with the other 1α,25-(OH)$_2$D$_3$ analogues, including **4b** (Figure 5A). A similar profile is observed at a dose of 1 nM, **4a** being more efficient compared to its parent analogue or 2α-methyl-1α,25(OH)$_2$D$_3$ (Figure 5A and not shown). Consistent with our previous findings, the antiproliferative effect of **4a** correlates with its capacity to better differentiate HL60 cells into monocyte-like cells compared to **2a** (Figure 5B). It should be emphasized that the 2α-methyl-1α,25(OH)$_2$D$_3$ has been reported to be between 2- and 4-fold more potent relative to 1α,25(OH)$_2$D$_3$ in inducing differentiation of HL60 cells, depending on the quantified parameter (nitroblue tetrazolium reduction assay

and CD11b surface cell marker expression).[21,32,33] However, no information of the concentration of the analogues used in these studies was provided. Our present data indicate that 1 nM 2α-methyl-1α,25(OH)$_2$D$_3$ was not sufficient to induce HL60 cells antiproliferation or differentiation (not shown). However, when used at the same low concentration, the C2α-methylated derivative of **2a** does achieve HL60 cell differentiation. This property is associated with a better binding affinity of **4a** for VDR compared to **2a** and 1α,25(OH)$_2$D$_3$, as evidenced by electrospray ionization mass spectrometry experiments (data not shown).

The in vitro biological data were not accompanied with a better capacity to reduce the serum calcium level in **4a**-treated mice. Nevertheless, we report that ip administration for 3 weeks of **4a** or **4b** every 2 days results in an optimal survival of mice, as no mice death was observed. Further dissociation between antiproliferative and calcemic effects has to be improved.

In summary, we have synthesized a novel 1α,25(OH)$_2$D$_3$ analogue, the 2α-methyl-20*S*,23*S*-epoxymethano-1α,25-dihydroxyvitamin D$_3$ (**4a**), which exhibits superagonistic and cellular antiproliferation/prodifferentiation properties while showing similar calcemic effects. In addition, its epimer **4b** (23*R*), which behaves like the natural ligand in vitro, is a noncalcemic vitamin D in vivo. To validate the potential application of these two analogues, further in vitro studies in distinct cell types are required to determine the specific gene activity and metabolic degradation.

Experimental Procedures

Chemistry. General. For general experimental procedures, see ref 19. CD-ring intermediates were named following the steroidal nomenclature.[34] Vitamin D analogues are named as vitamin D derivatives. IUPAC rules were used for the other compounds. In addition to NMR, HPLC analysis was used to determine the purity (>95%) of the vitamin D analogues.

Ethyl 8β-[(*tert*-Butyldimethylsilyl)oxy]-(20*R*,23)-epoxymethano-des-*A*,*B*-cholest-23*E*-en-25-oate (6a) and Ethyl 8β-[(*tert*-Butyldimethylsilyl)oxy]-(20*R*,23)-epoxymethano-des-*A*,*B*-cholest-23*Z*-en-25-oate (6b). A mixture of **6a** and **6b** (1.01 g), prepared by phosphonate chemistry,[19] was separated by HPLC (Phenomenex Silica(2), 250 mm × 21.2 mm, isocratic 3% EtOAc/hexanes) to give **6a** (*E*, 0.52 g, 46%, colorless oil) and **6b** (*Z*, 0.48 g, 42%, white solid, mp = 101 °C). Spectral data for the compounds **6a** and **6b** were identical to those reported.[19]

8β-[(*tert*-Butyldimethylsilyl)oxy]-(20*S*,23*S*)-epoxymethano-25-hydroxy-des-*A*,*B*-cholestane (9a) from 6a and 6b. PMHS [(poly(methylhydrosiloxane)] (0.11 mL, 1.82 mmol, 16 equiv) was added to a suspension of CuCl (8 mg, 0.08 mmol, 0.7 equiv), KO*t*-Bu (10 mg, 0.086 mmol, 0.75 equiv), and (*R*)-p-tolBINAP (9.3 mg, 0.014 mmol, 0.12 equiv) in hexanes (2 mL). The mixture was sonicated for 2 h. The color changed from yellow to deep-red. After the mixture was cooled to −25 °C, a solution of **6a** (50 mg, 0.114 mmol, 1 equiv) in hexanes (2 mL) and *i*-PrOH (0.035 mL, 0.456 mmol, 4 equiv) was added. After 1 h, the reaction was quenched by the addition of saturated NH_4Cl (5 mL) and EtOAc (5 mL). The mixture was extracted with EtOAc (2 × 10 mL), and the combined organic phase was dried, filtered, and concentrated in vacuo. The residue was dissolved in dry THF and cooled to −78 °C. After 15 min, a solution of MeLi in Et_2O (0.18 mL, 0.285 mmol, 1.6 M, 2.5 equiv) was added via syringe. The resulting solution was stirred for 5 min at −78 °C and then at room temp for 1 h. After the mixture was cooled to −78 °C, the reaction was quenched by the slow addition of saturated NH_4Cl (3 mL). The mixture was extracted with Et_2O (3 × 5 mL). The combined organic phase was dried, filtered, and concentrated in vacuo. The residue was purified by flash chromatography (SiO_2, 1.5 cm × 9 cm, 10% EtOAc/hexanes) to give **9a**[19] [45 mg, 92% (two steps), R_f = 0.2 (20% EtOAc/hexanes)]. Following a similar procedure, **9a** was also prepared from **6b** in 76% yield. Spectral data for the compound **9a** were identical to those reported.[19]

8*E*-Bromomethylene-(20*S*,23*S*)-epoxymethano-25-hydroxy-des-*A*,*B*-cholesta-8-one (10a). Sodium hexametildisilazide (0.75 mL, 1.5 mmol, 2 M, 3 equiv) was added to (bromomethylene)-triphenylphosphonium bromide (0.680 g, 1.56 mmol, 3.1 equiv) in 10 mL of THF at −60 °C. After 1 h, a solution of ketone **5a** (0.155 g, 0.502 mmol, 1 equiv) in THF (5 mL) was added via cannula. The solution was stirred at −60 °C for 5 min and then at room temperature for 3 h. Hexanes were added, and the suspension was filtered over a pad of silica gel (elution with 20% Et_2O/hexanes). After concentration in vacuo, the residue was purified by flash chromatography (SiO_2, 2 cm × 12 cm, 10% EtOAc/hexanes) to give the bromide **10a** [94 mg, 49%, colorless oil, R_f = 0.6 (50% EtOAc/ hexanes)]. ^{1}H NMR (250 MHz, $CDCl_3$): δ 5.61 (broad s, 1H, H-7), 4.09 (t, 1H, *J* = 7.9 Hz, H-28), 3.32 (t, 1H, *J* = 9.2 Hz, H-28), 2.83 (m, 1H, H-9), 2.45 (m, 1H, H-23), 1.22 (s, 3H, CH_3-21), 1.20 (s, 6H, CH_3-26 and CH_3-27), 0.66 (s, 3H, CH_3-18). ^{13}C NMR (62.9 MHz, $CDCl_3$): δ 144.8 (=C, C-8), 97.5 (=CH, C-7), 84.8 (C, C-20), 75.0 (CH_2, C-28), 70.7 (C, C-25), 59.0 (CH, C-17), 56.0 (CH, C-14), 46.3 (CH_2), 46.0 (CH_2), 45.5 (C, C-13), 40.0 (CH_2), 34.1 (CH, C-23), 30.9 (CH_2), 30.0 (CH_3, C-27), 29.7 (CH_3, C-26), 27.2 (CH_3, C-21), 22.5 (CH_2), 22.3 (CH_2), 21.7 (CH_2), 13.3 (CH_3, C-18).

8*E*-Bromomethylene-(20*S*,23*S*)-epoxymethano-25-[triethylsilyl]oxy]-des-*A*,*B*-cholestan-8-one (7a). Triethylsilyl chloride (0.140 mL, 0.84 mmol, 3 equiv) was added dropwise to a solution of alcohol **10a** (0.108, 0.280 mmol, 1 equiv), imidazol (0.06 g, 0.84 mmol, 3 equiv), and DMAP (0.007 g, 0.06 mmol, 0.2 equiv) in dry DMF (2 mL) at 0 °C. The cooling bath was removed, and the mixture was stirred for 12 h and poured onto a mixture of ice and saturated NH_4Cl (10 mL). The aqueous phase was extracted with hexanes (3 × 10 mL). The combined organic phase was dried, filtered, and concentrated in vacuo. The residue was purified by flash chromatography (SiO_2, 2 cm × 10 cm, 5% EtOAc/hexanes) to give **7a** [0.132 g, 94%, solid, R_f = 0.66 (10% EtOAc/hexanes). IR (dissolved in $CHCl_3$, cm^{-1}): 1630 ($\nu_{C=C}$). ^{1}H NMR (250 MHz, $CDCl_3$): δ 5.63 (broad s, 1H, H-7), 4.09 (t, 1H, *J* = 7.9 Hz, H-28), 3.32 (dd, 1H, J_1 = 9.7 Hz, J_2 = 8.6 Hz, H-28), 2.84 (m, 1H, H-9), 2.47 (m, 1H, H-23), 2.05 (d, 1H, *J* = 12.5 Hz, H-12), 1.97 (dd, 1H, J_1 = 11.9 Hz, J_2 = 7.3 Hz, H-14), 1.22 (s, 3H, CH_3-21), 1.20 (s, 6H, CH_3-26 and CH_3-27), 0.93 (t, 9H, *J* = 7.8 Hz, 3 × $C\underline{H}_3CH_2$-Si), 0.68 (s, 3H, CH_3-18), 0.55 (c, 6H, *J* = 7.8 Hz, 3 × $\underline{C}H_3C\underline{H}_2$-Si). ^{13}C NMR (62.9 MHz, $CDCl_3$): δ 144.9 (=C, C-8), 95.6 (=CH, C-7), 84.4 (C, C-20), 75.2 (CH_2, C-28), 73.1 (C, C-25), 59.1 (CH, C-17), 56.0 (CH, C-14), 47.9 (CH_2), 46.2 (CH_2), 45.5 (C, C-13), 40.0 (CH_2), 34.2 (CH, C-23), 30.9 (CH_2), 30.7 (CH_3, C-27), 30.0 (CH_3, C-26), 27.2 (CH_3, C-21), 22.6 (CH_2), 22.4 (CH_2), 21.7 (CH_2), 13.4 (CH_3, C-18), 7.1 (3 × CH_3, 3 × $\underline{C}H_3CH_2$-Si), 6.7 (3 × CH_2, 3 × $CH_3\underline{C}H_2$-Si). HMRS ([CI]$^+$): calculated for [$C_{26}H_{48}O_2Si^{79}Br$]$^+$ ([M + H]$^+$), 499.2607; found, 499.2609.

(1*R*,3*S*,4*R*,6*R*)-1,3-Dimethyl-4-(prop-1-en-2-yl)-7-oxa-bicyclo-[4.1.0]heptan-2-one (12). A solution of ketone **11** (10 g, 59.4 mmol, 1 equiv) in dry THF (50 mL) was added via syringe to a suspension of NaH (2.16 g, 89.1 mmol, 1.5 equiv) in THF (65 mL). After being stirred for 1 h, the mixture was cooled to 0 °C and then stirred for 10 min. MeI (4.5 mL, 72.3 mmol, 1.2 equiv) was added dropwise via syringe. The reaction mixture was stirred for 4 h. The reaction was quenched with saturated NH_4Cl (100 mL). The mixture was extracted with Et_2O (3 × 50 mL). The combined organic phase was dried, filtered, and concentrated. The residue was purified by MPLC (SiO_2, 5 cm × 45 cm, 3% EtOAc/hexanes) to give the monoalkylated compound **12** [5.03 g, 47%, colorless liquid, R_f = 0.37 (10% EtOAc/hexanes)]. Starting material recovered: 2.49 g (63% conversion). $[\alpha]_D^{25}$ 147 (*c* 2.4, $CHCl_3$). IR (neat, cm^{-1}): 1732

($\nu_{C=O}$), 1659 ($\nu_{C=C}$). ^{1}H NMR (400 MHz, $CDCl_3$): δ 4.81 (s, 1H, H-2′), 4.79 (s, 1H, H-2′), 3.40 (d, 1H, J = 3.1 Hz, H-6), 2.49 (td, 1H, J_1 = 11.9 Hz, J_2 = 4.2 Hz, H-4), 2.21 (dt, 1H, J_1 = 14.8 Hz, J_2 = 3.4 Hz, H-5), 1.97 (2H, m, H-3 and H-5), 1.63 (3H, s, CH_3-3′), 1.41 (3H, s, CH_3C-1), 1.04 (3H, d, J = 6.9 Hz, CH_3C-3). ^{13}C NMR (100.6 MHz, $CDCl_3$): 207.6 (C=O, C-2), 144.9 (=C, C-1′), 113.2 (=CH_2, C-2′), 60.6 (CH, C-6), 58.5 (C, C-1), 44.7 (CH, C-3), 42.2 (CH, C-4), 29.2 (CH_2, C-5), 18.4 (CH_3, C-3′), 15.8 (CH_3, CH_3C-1), 13.8 (CH_3, CH_3C-3). HMRS ([CI]$^+$): calculated for $[C_{11}H_{17}O_2]^+$ ([M + H]$^+$), 181.1228; found, 181.1222.

(1*R*,3*S*,4*R*,6*R*)-4-Hydroxy-1,3-dimethyl-7-oxabicyclo[4.1.0]heptan-one (13a). A stream of O_3/O_2 (0.7 bar, 0.1 NL/h, 50 w) was bubbled through a −78 °C cooled solution of ketone **12** (5 g, 27.74 mmol, 1 equiv) in dry MeOH (5.1 mL, 125 mmol, 4.5 equiv) and dry CH_2Cl_2 (50 mL) until the solution turned blue (30 min). The excess of O_3 was removed with a flow of argon for 30 min. The reaction mixture was allowed to reach room temperature (40 min) under a slow flow of argon and then cooled to −35 °C. After 10 min, Et_3N (30 mL, 222 mmol, 8 equiv) and DMAP (0.7 g, 5.6 mmol, 0.2 equiv) were successively and slowly added. Once DMAP has dissolved, Ac_2O (21 mL, 222 mmol, 8 equiv, freshly distilled from P_2O_5 under argon) was added. The reaction mixture was allowed to reach −8 °C and stirred for 2 h. The reaction was quenched by the slow addition of MeOH (20 mL). The mixture was stirred at room temperature for 5 min, diluted with EtOAc (100 mL), and successively washed with an aqueous solution of citric acid (2 × 50 mL, 10%) and saturated $NaHCO_3$ (2 × 50 mL). The combined organic phase was dried, filtered, and concentrated. The residue was dissolved in MeOH (60 mL). NaOAc (0.460 g, 5.55 mmol, 0.2 equiv) was added. The mixture was heated at 37 °C for 12 h and then concentrated to half volume. The residue was dissolved in EtOAc (30 mL) and washed with saturated NH_4Cl (25 mL). The aqueous phase was extracted with EtOAc (2 × 20 mL). The combined organic phase was dried, filtered, and concentrated. The residue was purified by flash chromatography (SiO_2, 5 cm × 10 cm, 20% EtOAc/hexanes) to give alcohol **13a** [3.47 g, 80%, colorless oil, R_f = 0.30 (50% EtOAc/hexanes)]. $[\alpha]_D^{25}$ 79.8 (c 1.3, $CHCl_3$). IR (neat, cm^{-1}): 3445 (ν_{O-H}), 1707 ($\nu_{C=O}$). ^{1}H NMR (400 MHz, $CDCl_3$): δ 3.79 (td, 1H, J_1 = 13.6 Hz, J_2 = 9.1 Hz, H-4), 3.38 (s, 1H, H-6), 2.62 (dt, 1H, J_1 = 14.4 Hz, J_2 = 3.6 Hz, H-5), 2.41 (s, 1H, OH), 2.01 (m, 1H, H-3), 1.92 (dd, 1H, J_1 = 14.4 Hz, J_2 = 10.0 Hz, H-5), 1.38 (s, 3H, CH_3C-1), 1.21 (d, 3H, J = 7.0 Hz, CH_3C-3). ^{13}C NMR (100.6 MHz, $CDCl_3$): δ 206.1 (C=O, C-2), 67.9 (CH, C-4), 59.9 (CH, C-6), 58.5 (C, C-1), 50.8 (CH, C-3), 32.1 (CH_2, C-5), 15.2 (CH_3, CH_3C-1), 12.5 (CH_3, CH_3C-3). Anal. Calcd for $[C_8H_{12}O_3]$: C, 62.06; H, 8.46. Found: C, 61.52; H, 7.94.

(1*R*,3*S*,4*R*,6*R*)-[(*tert*-Butyldimethylsilyl)oxy]-1,3-dimethyl-7-oxabicyclo[4.1.0]heptan-2-one (13b). Imidazole (2.6 g, 38.4 mmol, 2 equiv) and TBSCl (4.34 g, 28.8 mmol, 1.5 equiv) were successively added to a solution of alcohol **13a** (3 g, 19.2 mmol, 1 equiv) in dry DMF (30 mL). After 12 h, the reaction was quenched by the addition of a few pieces of ice and hexanes. The aqueous phase was extracted with hexanes (2 × 50 mL). The combined organic phase was dried, filtered, and concentrated. The residue was purified by flash chromatography (SiO_2, 4 cm × 10 cm, hexanes) to give **13b** [4.62 g, 89%, colorless oil, R_f = 0.75 (20% EtOAc/hexanes)]. $[\alpha]_D^{25}$ 24.2 (c 1.34, $CHCl_3$). IR (neat, cm^{-1}): 1712 ($\nu_{C=O}$). ^{1}H NMR (400 MHz, $CDCl_3$): δ 3.80 (td, 1H, J_1 = 9.0 Hz, J_2 = 4.8 Hz, H-4), 3.33 (dd, 1H, J_1 = 3.1 Hz, J_2 = 1.3 Hz, H-6), 2.49 (ddd, 1H, J_1 = 14.6 Hz, J_2 = 4.6 Hz, J_3 = 3.1 Hz, H-5), 2.06 (m, 1H, H-3), 1.9 (ddd, 1H, J_1 = 14.6 Hz, J_2 = 9.0 Hz, J_3 = 1.3 Hz, H-5), 1.38 (s, 3H, CH_3C-1), 1.14 (d, 3H, J = 7 Hz, CH_3C-3), 0.86 (s, 9H, Me_3C-Si), 0.06 (s, 3H, Me-Si), 0.04 (s, 3H, Me-Si). ^{13}C NMR (100.6 MHz, $CDCl_3$): δ 206.2 (C=O, C-2), 68.8 (CH, C-4), 60.1 (CH, C-6), 58.2 (C, C-1), 51.4 (CH, C-3), 32.8 (CH_2, C-5), 25.6 (3xCH_3, Me_3C-Si), 17.8 [C, (C, C-Si], 15.3 (CH_3, CH_3C-1), 12.8 (CH_3, CH_3C-3), −4.4 (CH_3, CH_3-Si), −4.8 (CH_3, CH_3-Si). HMRS ([CI]$^+$): calculated for $[C_{14}H_{27}O_3Si]^+$ ([M + H]$^+$), 271.1729; found, 271.1724.

(1*S*,2*S*,3*R*,4*R*,6*R*)-4-[(*tert*-Butyldimethylsilyl)oxy]-1,3-dimethyl-7-oxabicyclo[4.1.0]heptan-2-ol (14a). A solution of L-Selectride (22 mL, 22.2 mmol, 1 M, 1.5 equiv) in dry THF was added dropwise to a solution of ketone **13b** (4 g, 14.8 mmol, 1 equiv) in dry THF (40 mL) at −78 °C. After 30 min, the reaction was quenched by the dropwise addition of MeOH (10 mL) and H_2O (10 mL). A solution of NaOH (10 mL, 10%) and H_2O_2 (10 mL, 30% v/v) was successively and slowly added. The mixture was allowed to reach room temperature over 12 h. A saturated solution of NH_4Cl (30 mL) was added. The aqueous phase was extracted with a solution of EtOAc/hexanes (20%, 3 × 50 mL). The combined organic phase was dried, filtered, and concentrated. The residue was purified by flash chromatography (SiO_2, 4 cm × 10 cm, 20% EtOAc/hexanes) to give **14a** [3.51 g, 87%, colorless, R_f = 0.4 (20% EtOAc/hexanes)]. $[\alpha]_D^{25}$ −79.7 (c 3.7, $CHCl_3$). IR (neat, cm^{-1}): 3471 (ν_{O-H}). ^{1}H NMR (400 MHz, $CDCl_3$): δ 3.82 (dd, 1H, J_1 = 10.3 Hz, J_2 = 4.5 Hz, H-2), 3.51 (td, 1H, J_1 = 9.0 Hz, J_2 = 4.6 Hz, H-4), 3.24 (sa, 1H, H-6), 2.37 (dd, 1H, J_1 = 14.8 Hz, J_2 = 4.5 Hz, H-5), 1.81 (d, 1H, J = 10.3 Hz, OH), 1.66 (dd, 1H, J_1 = 14.8 Hz, J_2 = 9.0 Hz, H-5), 1.49 (m, 1H, H-3), 1.42 (s, 3H, CH_3C-1), 0.98 (d, 3H, J = 7.0 Hz, CH_3C-3), 0.87 (s, 9H, Me_3C-Si), 0.04 (s, 3H, CH_3-Si), 0.03 (s, 3H, Me-Si). ^{13}C NMR (100.6 MHz, $CDCl_3$): δ 72.8 (CH, C-2), 66.3 (CH, C-4), 63.7 (CH, C-6), 60.9 (C, C-1), 42.2 (CH, C-3), 34.9 (CH_2, C-5), 25.8 (3 × CH_3, Me_3C-Si), 21.6 (CH_3, CH_3C-1), 18.0 (C, C-Si), 12.4 (CH_3, CH_3C-3), −4.4 (CH_3, Me-Si), −4.8 (CH_3, Me-Si). Anal. Calcd for $[C_8H_{12}O_3]$: C, 61.72; H, 10.36. Found: C, 61.93; H, 10.49.

(1*R*,2*S*,3*S*,4*R*,6*R*)-2,4-Bis[(*tert*-butyldimethylsilyl)oxy)-1,3-dimethyl-7-oxabicyclo[4.1.0]heptane (14b). Imidazole (0.63 g, 9.2 mmol, 2.5 equiv) and TBSCl (1.1 g, 7.34 mmol, 2 equiv) were successively added to a solution of alcohol **14a** (1 g, 3.67 mmol, 1 equiv) in dry DMF (10 mL). After 12 h, the reaction was quenched by the addition of ice pieces and saturated NH_4Cl (10 mL). The aqueous phase was extracted with hexanes (3 × 15 mL). The combined organic phase was dried, filtered, and concentrated in vacuo. The residue was purified by flash chromatography (SiO_2, 3 cm × 10 cm, hexanes) to give **14b** [1.37 g, colorless oil, R_f = 0.78 (20% EtOAc/hexanes)]. $[\alpha]_D^{25}$ −42.3 (c 4.2, $CHCl_3$). ^{1}H NMR (400 MHz, $CDCl_3$): δ 4.22 (d, 1H, J = 5.7 Hz, H-2), 3.79 (td, 1H, J_1 = 9.1 Hz, J_2 = 4.4 Hz, H-4), 2.97 (d, 1H, J = 4.5 Hz, H-6), 2.19 (dd, 1H, J_1 = 15.5 Hz, J_2 = 4.1 Hz, H-5), 1.84 (m, 1H, H-3), 1.71 (dt, 1H, J_1 = 15.5 Hz, J_2 = 4.2 Hz, H-5), 1.32 (s, 3H, CH_3C-1), 0.94 (s, 9H, Me_3C-Si), 0.93 (d, 3H, J = 6.8 Hz, CH_3C-3), 0.88 (s, 9H, Me_3C-Si), 0.11 (s, 3H, Me-Si), 0.07 (s, 3H, Me-Si), 0.03 (s, 6H, 2 × Me-Si). ^{13}C NMR (100.6 MHz, $CDCl_3$): δ 71.2 (CH, C-2), 70.5 (CH, C-4), 59.8 (C, C-1), 59.5 (CH, C-6), 41.5 (CH, C-3), 31.1 (CH_2, C-5), 25.9 (3 × CH_3, Me_3C-Si), 25.7 (3 × CH_3, Me_3C-Si), 21.4 (CH_3, CH_3C-1), 18.3 (C, C-Si), 17.9 (C, C-Si), 11.7 (CH_3, CH_3C-3), −4.5 (CH_3, Me-Si), −4.6 (CH_3, Me-Si), −4.8 (CH_3, Me-Si), −4.9 (CH_3, Me-Si). Anal. Calcd for $[C_{20}H_{43}O_3Si_2]$: C, 62.12; H, 10.95. Found: C, 62.36; H, 11.26.

(3*R*,4*S*,5*S*)-3,5-Bis[(*tert*-butyldimethylsilyl)oxy]-4-methyl-6-oxoheptanal (15). H_5IO_6 (2.65 g, 11.64 mmol, 3 equiv) was added to a solution of epoxide **14b** (1.5 g, 3.73 mmol, 1 equiv) in dry Et_2O (20 mL). After 12 h, the reaction mixture was poured into an aqueous saturated solution of $Na_2S_2O_3$ (20 mL). The aqueous phase was extracted with Et_2O (3 × 15 mL). The combined organic phase was dried, filtered, and concentrated in vacuo to give aldehyde **11** (1.56 g), which was immediately used in the next step. ^{1}H NMR (250 MHz, $CDCl_3$): δ 9.71 (t, 1H, J = 2.4 Hz, H-1), 4.17 (c, 1H, J = 5.4 Hz, H-3), 3.88 (d, 1H, J = 5.1 Hz, H-5), 2.65 (m, 2H, CH_2-4), 2.10 (s, 3H, CH_3-7), 1.93 (m, 1H, H-4), 0.86 (s, 9H, Me_3C-Si), 0.80 (d, 3H, J = 7.0 Hz, CH_3C-4), 0.79 (s, 9H, Me_3C-Si), −0.01 (s, 3H, Me-Si), −0.02 (s, 3H, Me-Si), −0.03 (s, 3H, Me-Si), −0.04 (s, 3H, Me-Si). ^{13}C NMR (62.9 MHz, $CDCl_3$): δ 211.4 (C=O, C-6), 201.9 (C=O, C-1), 79.9 (CH, C-5), 69.0 (CH, C-3), 48.9 (CH_2, C-2), 44.0 (CH, C-4), 26.6 (CH_3, C-7),

25.7 (3 × CH_3, Me_3C-Si), 25.6 (3 × CH_3, Me_3C-Si), 17.9 (C, C-Si), 17.8 (C, C-Si), 12.5 (CH_3, CH_3C-4), −3.7 (CH_3, Me-Si), −4.6 (CH_3, Me-Si), −5.1, (CH_3, Me-Si), −5.2 (CH_3, Me-Si).

(3*S*,4*S*,5*R*)-3,5-Bis[(*tert*-butyldimethylsilyl)oxy]-8,8-dibromo-4-methyloct-7-en-2-one (16). CBr_4 (3.86 g, 11.64 mmol, 3 equiv) was added to a suspension of Ph_3P (3.05 g, 11.64 mmol, 3 equiv) and Zn (0.761 g, 11.64 mmol, 3 equiv) in CH_2Cl_2 (15 mL) at 0 °C. After 5 min, the cooling bath was removed and the reaction mixture was stirred at room temperature for 2 h. The color changed from green to deep-red. A solution of aldehyde **15** (1.56 g, 4.88 mmol, 1 equiv) in CH_2Cl_2 (5 mL) was added via cannula. After 45 min, the reaction mixture was filtered through a path of silica gel (elution with hexanes and 20% EtOAc/hexanes). After concentration in vacuo, the residue was purified by flash chromatography (SiO_2, 3 cm × 12 cm, 2% EtOAc/hexanes) to give the dibromide **16** [1.63 g, 75% (two steps), colorless oil, R_f = 0.50 (5% EtOAc/hexanes). $[\alpha]_D^{25}$ −25.4 (*c* 2.0, $CHCl_3$). IR (neat, cm^{-1}): 1708 ($\nu_{C=O}$), 1633 ($\nu_{C=C}$). ^1H NMR (400 MHz, $CDCl_3$): δ 6.46 (dd, 1H, J_1 = 8.1 Hz, J_2 = 5.9 Hz, H-7), 3.88 (d, 1H, J = 5.6 Hz, H-3), 3.83 (c, 1H, J = 5.4 Hz, H-5), 2.59 (ddd, 1H, J_1 = 15.5 Hz, J_2 = 8.2 Hz, J_3 = 5.1 Hz, H-6), 2.3 (dt, 1H, J_1 = 15.5 Hz, J_2 = 5.7 Hz, H-6), 2.17 (s, 3H, CH_3-1), 1.81 (m, 1H, H-4), 0.94 (s, 9H, Me_3C-Si), 0.89 (d, 3H, J = 5.5 Hz, CH_3C-4), 0.88 (s, 9H, Me_3C-Si), 0.08 (s, 3H, Me-Si), 0.06 (s, 3H, Me-Si), 0.04 (s, 6H, 2 × Me-Si). ^{13}C NMR (100.6 MHz, $CDCl_3$): δ 212.3 (C=O, C-2), 135.5 (CH, C-7), 90.0 (C, C-8), 79.6 (CH, C-3), 71.2 (CH, C-5), 43.6 (CH, C-4), 38.8 (CH_2, C-6), 27.0 (CH_3, C-1), 25.9 (3 × CH_3, Me_3C-Si), 25.7 (3 × CH_3, Me_3C-Si), 18.1 (C, C-Si), 18.0 (C, C-Si), 11.8 (CH_3, CH_3-C-4), −4.2 (CH_3, Me-Si), −4.4 (CH_3, Me-Si), −4.8 (CH_3, Me-Si), −4.9 (CH_3, Me-Si). HMRS ($[CI]^+$): calculated for $[C_{21}H_{43}Br_2O_3Si]^+$, 557.1117; found, 557.1115.

(3*S*,4*S*,5*R*)-3,5-Bis[(*tert*-butyldimethylsilyl)oxy]-4-methyloct-1-en-7-yne-2-yl Trifluoromethanesulfonate (8). A freshly prepared solution of LiN(*i*-Pr)$_2$ in THF (6 mL, 0.9 M, 3 equiv) was added dropwise to a solution of the dibromide **16** (1 g, 1.79 mmol, 1 equiv) in THF (10 mL) at −78 °C. After being stirred for 1 h, a solution of *n*-BuLi in hexanes (0.25 mL, 0.54 mmol, 2.5 M, 0.3 equiv) was added. After 15 min, *N*-(5-chloro-2-pyridyl)bis-(trifluoromethanesulfonimide) (2.1 g, 5.37 mmol, 3 equiv) was added at once. The reaction mixture was allowed to reach room temperature over 12 h. The reaction was quenched by the addition of saturated NaCl (20 mL). The aqueous phase was extracted with Et_2O (2 × 20 mL). The combined organic phase was dried, filtered, and concentrated in vacuo. The residue was purified by flash chromatography (SiO_2, 3 cm × 12 cm, hexanes) to give enoltriflate **8** [0.712 g, 75%, colorless oil, R_f = 0.75 (5% Et_2O/hexanes)]. $[\alpha]_D^{25}$ −1.52 (*c* 2.1 mg/mL, $CHCl_3$). IR (neat, cm^{-1}): 3312 ($\nu_{\equiv C-H}$), 1663 ($\nu_{C=C}$). ^1H NMR (500 MHz, $CDCl_3$): δ 5.24 (d, 1H, J = 3.7 Hz, H-1), 5.15 (d, 1H, J = 3.7 Hz, H-1), 4.10 (d, 1H, J = 7.3 Hz, H-3), 4.07 (ddd, 1H, J_1 = 7.4 Hz, J_2 = 5.3 Hz, J_3 = 3.2 Hz, H-5), 2.43 (ddd, 1H, J_1 = 16.8 Hz, J_2 = 5.3 Hz, J_3 = 2.7 Hz, H-6), 2.38 (ddd, 1H, J_1 = 1.7 Hz, J_2 = 7.5 Hz, J_3 = 2.7 Hz, H-6), 2.12 (cd, 1H, J_1 = 7.1 Hz, J_2 = 3.2 Hz, H-4), 1.99 (t, 1H, J = 2.7 Hz, H-8), 0.92 (s, 9H, Me_3C-Si), 0.89 (s, 9H, Me_3C-Si), 0.87 (d, 3H, J = 7.0 Hz, CH_3C-4), 0.11 (CH_3, Me-Si), 0.10 (CH_3, Me-Si), 0.09 (CH_3, Me-Si), 0.08 (CH_3, Me-Si). ^{13}C NMR (125.7 MHz, $CDCl_3$): δ 156.2 (=C, C-2), 118.4 (C, c, J = 320 Hz, CF_3), 104.4 (=CH_2, C-1), 80.8 (≡CH, C-8), 74.1 (CH, C-3), 70.7 (≡C, C-7), 70.1 (CH, C-3), 42.1 (CH, C-4), 25.8 (3 × CH_3, Me_3C-Si), 25.7 (3 × CH_3, Me_3C-Si), 25.7 (CH_2, C-6), 18.2 (C, C-Si), 18.1 (C, C-Si), 9.8 (CH_3, CH_3C-4), −3.8 (CH_3, Me-Si), −4.4 (CH_3, Me-Si), −5.0 (2 × CH_3, 2 × Me-Si). HMRS ($[CI]^+$): calculated for $[C_{22}H_{42}F_3O_5SSi_2]^+$, 531.2244; found, 531.2239.

2α-Methyl-20*S*,23*S*-epoxymethano-1α,25-dihydroxyvitamin D$_3$ (4a). A solution of *t*-BuLi in pentane (0.280 mL, 0.427 mmol, 1.55 M, 2.2 equiv) was added dropwise to a solution of bromide **7a** (0.097 g, 0.194 mmol, 1 equiv) in dry THF (2 mL) at −78 °C. After the mixture was stirred for 1 h, a solution of dry $ZnBr_2$ in THF (0.46 mL, 0.232 mmol, 0.5 M, 1.2 equiv) was added dropwise. After 5 min, the −78 °C cooling bath was replaced by an ice−water cooling bath and the yellow solution was stirred for 1 h. A solution of enoltriflate **8** (0.070 g, 0.132 mmol, 0.68 equiv), $(Ph_3P)_4Pd$ (15 mg, 0.012 mmol, 6 mol %), and dry Et_3N (0.1 mL, 0.75 mmol, 4 equiv) in dry THF (2 mL) was added. The yellow color changed to orange. The reaction mixture was stirred in the dark for 5 min at 0 °C and then at room temperature for 12 h. The reaction was quenched by the addition of H_2O (1 mL). The aqueous phase was extracted with Et_2O (3 × 3 mL). The combined organic phase was dried, filtered, and concentrated in vacuo. The residue (**17a**) was dissolved in THF (2 mL) under argon. A solution of *n*-Bu_4NF in THF (1 mL, 0.97 mmol, 1 M, 5 equiv) was added. The mixture was stirred for 24 h. The reaction was quenched by the addition of saturated NH_4Cl (5 mL). The aqueous phase was extracted with EtOAc (3 × 10 mL). The combined organic phase was dried, filtered, and concentrated in vacuo. The residue was purified by flash chromatography (SiO_2, 1.5 cm × 10 cm, 50% EtOAc/hexanes) to give **4a** [0.033 g, 55%, white solid, R_f = 0.48 (60% EtOAc/hexanes)]. ^1H NMR (500 MHz, $CDCl_3$): δ 6.37 (d, 1H, J = 11.3 Hz, H-6), 6.01 (d, 1H, J = 11.3 Hz, H-7), 5.27 (s, 1H, H-19), 5.00 (d, 1H, J = 1.6 Hz, H-19), 4.31 (d, 1H, J = 3.1 Hz, H-1), 4.10 (t, 1H, J = 7.9 Hz, H-28), 3.84 (td, 1H, J_1 = 7.5 Hz, J_2 = 4.3 Hz, H-3), 3.34 (dd, 1H, J_1 = 9.7 Hz, J_2 = 8.5 Hz, H-28), 2.81 (d, 1H, J_1 = 12.5 Hz, H-9), 2.66 (dd, 1H, J_1 = 13.5 Hz, J_2 = 3.8 Hz, H-4), 2.46 (m, 1H, H-23), 2.22 (dd, 1H, J_1 = 13.5 Hz, J_2 = 7.6 Hz, H-4), 2.05 (d, 1H, J = 11.7 Hz, H-12), 1.99 (dd, 1H, J_1 = 11.2 Hz, J_2 = 7.9 Hz, H-14), 1.92 (cd, 1H, J_1 = 7.0 Hz, J_2 = 3.7 Hz, H-2), 1.23 (s, 3H, CH_3-21), 1.22 (s, 6H, CH_3-26 and CH_3-27), 1.06 (d, 3H, J = 6.9 Hz, CH_3C-2α), 0.66 (s, 3H, CH_3-18). ^{13}C NMR (125.7 MHz, $CDCl_3$): δ 146.5 (=C, C-10), 142.7 (=C, C-8), 133.1 (=C, C-5), 124.7 (=CH, C-6), 117.3 (=CH, C-7), 113.1 (=CH_2, C-19), 84.9 (C,C-20), 75.2 (CH, C-1), 73.2 (CH_2, C-28), 71.7 (CH, C-3), 70.9 (CH, C-25), 59.8 (CH, C-14), 56.5 (CH, C-17), 47.1 (CH2, C-22), 46.9 (CH_2, C-24), 46.1 (C, C-13), 44.1 (CH_2, C-2), 43.2 (CH_2, C-4), 40.7 (CH_2, C-12), 35.9 (CH, C-23), 30.2 (CH_3, C-27), 29.7 (CH_3, C-26), 29.0 (CH_2, C-9), 27.6 (CH_3, CH_3-21), 23.4 (CH_2), 22.7 (CH_2), 21.9 (CH_2), 13.2 (CH_3, C-18), 12.4 (CH_3, CH_3C-2α). HMRS (ESI-TOF): calculated for $[C_{29}H_{47}O_4]^+$ ([M + H]$^+$), 459.3475; found, 459.3469.

2α-Methyl-20*S*,23*R*-epoxymethano-1α,25-dihydroxyvitamin D$_3$ (4b). A solution of *t*-BuLi in pentane (0.370 mL, 0.630 mmol, 1.7 M, 2.1 equiv) was added dropwise to a solution of bromide **7b** (0.150 g, 0.3 mmol, 1 equiv) in dry THF (2 mL) at −78 °C. After the mixture was stirred for 1 h, a solution of dry $ZnBr_2$ in THF (0.5 mL, 0.41 mmol, 0.82 M, 1.37 equiv) was added dropwise. After 5 min, the −78 °C cooling bath was replaced by an ice−water cooling bath and the yellow solution was stirred for 1 h. A solution of enoltriflate **8** (0.080 g, 0.150 mmol, 0.5 equiv), $(Ph_3P)_4Pd$ (20 mg, 0.017 mmol, 6 mol %), and dry Et_3N (0.2 mL, 1.5 mmol, 5 equiv) in dry THF (2 mL) was added. The yellow color changed to orange. The reaction mixture was stirred in the dark for 5 min at 0 °C and then at room temperature for 6 h. The reaction was quenched by the addition of H_2O (1 mL). The aqueous phase was extracted with Et_2O (3 × 3 mL). The combined organic phase was dried, filtered, and concentrated in vacuo. The residue (**17b**) was dissolved in a mixture of deoxygenated CH_2Cl_2 (2 mL), CH_3CN (2 mL), and Et_3N (1 mL). HF−Py complex (0.2 mL) was added. The mixture was stirred at room temperature for 2 h. The reaction was quenched by the addition of saturated $NaHCO_3$ (5 mL). The aqueous phase was extracted with EtOAc (3 × 10 mL). The combined organic phase was dried, filtered, and concentrated in vacuo. The residue was purified by flash chromatography (SiO_2, 1.5 cm × 10 cm, 50% EtOAc/hexanes) and then by HPLC (Phenomenex Silica(2), 250 mm × 1.2 mm, 10% *i*-PrOH/hexanes) to give **4b** [0.036 g, 53%, white solid, R_f = 0.48 (60% EtOAc/hexanes)]. ^1H NMR (500 MHz, $CDCl_3$): δ 6.37 (d, 1H, J = 11.3 Hz, H-6), 6.00 (d, 1H, J = 11.3 Hz, H-7), 5.27 (s, 1H, H-19), 5.00 (d, 1H, J = 1.9 Hz, H-19), 4.31 (d, 1H, J = 3.6 Hz,

H-1), 4.07 (t, 1H, J = 7.7 Hz, H-28), 3.84 (td, 1H, J_1 = 7.5 Hz, J_2 = 4.2 Hz, H-3), 3.37 (dd, 1H, J_1 = 9.8 Hz, J_2 = 8.9 Hz, H-28), 2.81 (dd, 1H, J_1 = 11.9 Hz, J_2 = 3.7 Hz, H-9), 2.66 (dd, 1H, J_1 = 13.6 Hz, J_2 = 3.9 Hz, H-4), 2.32 (m, 1H, H-23), 1.27 (s, 3H, CH_3-21), 1.21 (s, 6H, CH_3-26 and CH_3-27), 1.06 (d, 3H, J = 6.9 Hz, CH_3C-2), 0.66 (s, 3H, CH_3-18). ^{13}C NMR (125.7 MHz, $CDCl_3$): δ 146.5 (=C, C-10), 142.7 (=C, C-8), 133.1 (=C, C-5), 124.7 (=CH, C-6), 117.3 (=CH, C-7), 113.1 ($=CH_2$, C-19), 84.9 (C,C-20), 75.2 (CH, C-1), 73.2 (CH_2, C-28), 71.7 (CH, C-3), 70.9 (CH, C-25), 59.8 (CH, C-14), 56.5 (CH, C-17), 47.1 (CH_2, C-22), 46.9 (CH_2, C-24), 46.1 (C, C-13), 44.1 (CH_2, C-2), 43.2 (CH_2, C-4), 40.7 (CH_2, C-12), 35.9 (CH, C-23), 30.2 (CH_3, C-27), 29.7 (CH_3, C-26), 29.0 (CH_2, C-9), 27.6 (CH_3, CH_3-21), 23.4 (CH_2), 22.7 (CH_2), 21.9 (CH_2), 13.2 (CH_3, C-18), 12.4 (CH_3, CH_3C-2α). HMRS (ESI-TOF): calculated for $[C_{29}H_{47}O_4]^+$ ($[M + H]^+$), 459.3475; found, 459.3478.

Purification and Crystallization. Purification and crystallization of the human VDR LBD complexes with **4a** or **4b** were performed as previously described.[6] The LBD of the human VDR (residues 118−427, Δ166−216) was cloned in pET28b expression vector to obtain an N-terminal hexahistidine-tagged fusion protein and was overproduced in *E. coli* BL21 (DE3) strain. Cells were grown in Luria−Bertani medium and subsequently incubated for 3 h at 25 °C with 1 mM isopropyl thio-β-D-galactoside. The protein purification included a metal affinity chromatography step on a cobalt-chelating resin (TALON, Clontech). The tag was removed by thrombin digestion overnight at 4 °C, and the protein was further purified by gel filtration on a Superdex S200 16/60 column (Amersham). The protein buffer prior to concentration of the protein contains 20 mM Tris, pH 7.5, 200 mM NaCl, and 2 nM TCEP. The protein was concentrated to 3.5 mg/mL and incubated in the presence of a 1.5-fold excess of ligands. The purity and homogeneity of the protein were assessed by SDS−PAGE. Crystals of complexes were obtained at 4 °C by vapor diffusion method using crystals of VDR LBD/1α,25(OH)$_2$D$_3$ as microseeds. The reservoir solution contained 0.1 M Mes and 1.4 M ammonium sulfate at pH 6.0.

X-ray Data Collection and Structure Determination. The crystals were mounted in fiber loop and flash-cooled in liquid nitrogen after cryoprotection with a solution containing the reservoir solution plus 30% glycerol and 2% polyethylene glycol 400. Data collection from a single frozen crystal was performed at 100 K on beamlines ID23-2 and ID29 of the ESRF (Grenoble, France) for **4a** and **4b** complexes, respectively. The crystals belong to the orthorhombic space group $P2_12_12_1$ with one monomer per asymmetric unit. Data were integrated and scaled using HKL2000.[35] A rigid body refinement was used with the structure of the hVDR LBD/1α,25(OH)$_2$D$_3$ complex as a starting model. Refinement involved iterative cycles of manual building and refinement calculations. The programs Refmac[36] and COOT[37] were used throughout structure determination and refinement. The ligand molecule was included only at the last stage of the refinement. The omit map from the refined atomic model of VDR LBD was used to fit the ligand to its electron density, shown in Figure 2A. Anisotropic scaling and a bulk solvent correction were used. Individual B atomic factors were refined isotropically for the **4a** complex and anisotropically for the **4b** complex. Solvent molecules were then placed according to unassigned peaks in the difference Fourier map. In the VDR/**4a** complex, refined at 1.7 Å with no σ cutoff, the final model consists of residues 118−423 (Δ166−216), the ligand, two sulfate ions, and 447 water molecules. In the VDR/**4b** complex refined at 1.45 Å with no σ cutoff, the final model consists of residues 118−423 (Δ166−216), the ligand, two sulfate ions, and 458 water molecules. According to PROCHECK,[38] 93.0% of peptide lies in the most favored regions and 7.0% in additional allowed regions for the VDR/**4a** complex, and 93.4% of peptide lies in most favored regions and 6.6% in additional allowed regions for the VDR/**4b** complex. Data are summarized in Supporting Information Table 1. The volumes of each ligand binding pocket and each ligand were calculated as previously reported.

Steady-State Fluorescence Anisotropy Measurements. Steady-state anisotropy measurements were performed with a T-format SLM 8000 spectrofluorometer. Anisotropy titrations were carried out by adding increasing hVDR LBD concentrations to 1 μM fluorescent labeled TAMRA (tetramethylrhodamine)-SRC-1 (RHKILHRLLQEGSPS) peptide in 20 mM Tris-HCl (pH 7.5), 200 mM NaCl. The binding affinity constants of the SRC-1 peptide to hVDR LBD was determined in response to 1α,25(OH)$_2$D$_3$, **2a**, **4a**, or **4b**. The excitation wavelength was 550 nm, and the emitted light was monitored through high-pass filters (550 nm) (Kodak). A home-built device ensured the automatic rotation of the excitation polarizer. Assuming that hVDR binds with the TAMRA-SRC-1 peptide in a 1:1 stoichiometry, the model used to describe the binding experiment was the following:

$$R + L \overset{K_d}{\leftrightarrow} P$$

L and R represent the hVDR LBD and the TAMRA-SRC-1 peptide, respectively, and P designates the hVDR LBD/TAMRA-SRC-1 complex.

The Scatchard equation was rewritten to fit the anisotropy, r, as follows:

$$r = r_0 + (r_f - r_0)\left(\frac{(Rt + Lt + K_d) - \sqrt{(Rt + Lt + K_d)^2 - 4\,Rt\,Lt}}{2\,Rt}\right)$$

Lt and Rt are the total concentrations of hVDR LBD and TAMRA-SRC-1 peptides, respectively; r_f represents the anisotropy at the plateau when all the complex is formed, whereas r_0 and r correspond to the anisotropy values of the TAMRA-SRC-1 peptide in the absence and in the presence of a given concentration of hVDR, respectively. K_d corresponds to the dissociation constant of the complex. All experiments were performed at 20 °C, and results are representative of three distinct experiments.

Transient Transfections and Luciferase Reporter Gene Assays. The chimera Gal4-VDR LBD (90−427) was constructed by PCR using the appropriate oligonucleotides with restriction sites (XhoI/*Bam*HI) and the pSG5 VDR plasmid (1−427) as template and cloned into the vector PXJ440 encoding the DBD of the yeast activator Gal4 (1−147). MCF-7 human breast cancer cells were seeded into 24-well plates (10^5 cells per well) and grown overnight in phenol red-free Dulbecco's modified Eagle's medium (DMEM) supplemented with 10% charcoal-treated fetal bovine serum (FCS), 5% gentamycin, and 0.6 μg/mL insulin. Liposomes were formed using the transfection reagent jetPEI (Polyplus transfection) and used according to the manufacturer's instructions. Cells were transfected with 25 ng of the expression plasmid pXJ440-Gal$_4$DBD-hVDR (90−427), 250 ng of the reporter plasmid ptk-LUC, 50 ng of the pCH110-β-galactosidase vector (used as an internal control to normalize variation in transfection efficiency), and 675 ng of the carrier plasmid pBluescript (Stratagene). Ten hours later, cells were washed with freshly prepared phosphate buffered saline (PBS) and various concentrations of 1α,25(OH)$_2$D$_3$, **4a**, **4b**, **2a**, and **2b** versus control (solvent) were added to the cells in phenol red-free DMEM supplemented with 10% FCS. Twenty-four hours after the onset of stimulation, cells were rinsed in PBS and lysed in 100 μL of reporter gene lysis buffer (Roche Diagnostics). Cell extracts were assayed for luciferase and β-galactosidase activities. Luciferase reporter activity was determined by using luciferin as the substrate, and β-galactosidase activity was measured using *o*-nitrophenyl-β-galactoside as the substrate. The chemiluminescence from activated luciferin was measured on a luminometer plate reader LB96P (Berthold

Technologies). Luciferase values were normalized to the β-galactosidase activity. Luciferase activities are expressed as arbitrary units of light intensity. Data points represent the mean of assays performed in triplicate for at least three independent experiments. For every triplicate, the mean and the standard deviation of the mean were calculated.

HL60 Cell Culture and Differentiation. HL60 cells were cultured in complete RPMI with 10% fetal calf serum (Sigma) and 5% gentamycine (Kalys) at 37 °C without CO_2 as previously described.[19] Cells were plated at a density of 4×10^5 cells/mL and cultured for 96 h in the presence of 1α,25$(OH)_2D_3$, **2a**, or **4a** and **4b** at various concentrations. Control incubations were performed with 0.7% ethanol. HL60 cell differentiation was determined by flow cytometry using PE-conjugated antihuman CD11c and FITC-conjugated antihuman CD14 antibodies (Pharmingen/BD Biosciences). Topro-3 (Molecular probes) was added immediately before laser excitation to exclude dead cells. Cells were analyzed on a FACSCalibur (Becton Dickinson) and using the FlowJo (TreeStar Inc.) software.

Mice and Serum Calcium Quantitation. Animal protocols were approved by the Alsace Regional Ethics Committee. Male C57BL/6J mice were obtained from Charles River Laboratories, France (L'Arbresle, France). Mice (6−7 weeks old) were maintained in a temperature-controlled (23 °C) facility with a 12 h light/dark cycle and were given free access to food and water. Mice were fed with the standard mouse chow (D03 SAFE; Augy, France) and tap water. The different 1α,25$(OH)_2D_3$ agonists were dissolved in sesame oil and administered intraperitoneally every 2 days at a dose of 0.1 μg/kg. Mice were fasted 3 h prior to blood harvest, and subsequent calcium measurements were determined with a kit supplied by Olympus according to the manufacturer's procedure on an Olympus AU400 analyzer (Olympus SA, Ringis, France).[39]

Acknowledgment. We thank the beamline staff at the ESRF (Grenoble, France) for help during data collection. The study described here was supported by CNRS, INSERM, ULP, the European Commission as SPINE2 complexes (Contract No. LSHG-CT-2006-031220) under the RDT programme "Quality of Life and Management of Living Resources", the Spanish MEC (Grants SAF2004-01885 and SAF2007-67205), and Xunta de Galicia (Grants INCITE08P-XIB-209130PR and ACEUIC-2006/XA050). The authors are grateful to Jean-Marc Bornert, Cindy Vincent, and Magali Huc for mouse experiments, to the clinical biochemistry team of the Mouse Clinics Institute for serum calcium measurements, and to Dr. Daniel Metzger for helpful discussions. We thank Yves Mély for advice with fluorescence experiments. We thank Claudine Ebel and Sara Milosevic for advice with flow cytometry experiments and the cytometry common service. R. S. thanks the Spanish MEC for a FPI grant and T.H. for a fellowship from the Regional Council of Alsace. The authors declare that they have no competing financial interests.

Supporting Information Available: Table 1 listing crystallographic data and refinement statistics, experimental procedures for the chemical synthesis, and NMR spectra of compounds. This material is available free of charge via the Internet at http://pubs.acs.org.

References

(1) Jensen, E. V. From chemical warfare to breast cancer management. *Nat. Med.* **2004**, *10*, 1018–1021.
(2) Evans, R. M. A transcription basis for physiology. *Nat. Med.* **2004**, *10*, 1022–1026.
(3) Chambon, P. How I became one of the fathers of a superfamily. *Nat. Med.* **2004**, *10*, 1027–1031.
(4) Bourguet, W.; Ruff, M.; Chambon, P.; Gronemeyer, H.; Moras, D. Crystal structure of the ligand-binding domain of the human nuclear receptor RXR-alpha. *Nature* **1995**, *375*, 377–382.
(5) Renaud, J. P.; Rochel, N.; Ruff, M.; Vivat, V.; Chambon, P.; Gronemeyer, H.; Moras, D. Crystal structure of the RAR-gamma ligand-binding domain bound to all-trans retinoic acid. *Nature* **1995**, *378*, 681–689.
(6) Rochel, N.; Wurtz, J. M.; Mitschler, A.; Klaholz, B.; Moras, D. The crystal sructure of the nuclear receptor for vitamin D bound to its natural ligand. *Mol. Cell* **2000**, *5*, 173–179.
(7) Bouillon, R.; Eelen, G.; Verlinden, L.; Mathieu, C.; Carmeliet, G.; Verstuyf, A. Vitamin D and cancer. *J. Steroid Biochem. Mol. Biol.* **2006**, *102*, 156–162.
(8) Hendy, G. N.; Hruska, K. A.; Mathew, S.; Goltzman, D. New insights into mineral and skeletal regulation by active forms of vitamin D. *Kidney Int.* **2006**, *69*, 218 223.
(9) Christakos, S.; Dhawan, P.; Benn, P.; Porta, A.; Hediger, M.; Oh, G. T.; Jeung, E. B.; Zhong, Y.; Ajibade, D.; Dhawan, K.; Joshi, J. Vitamin D: molecular mechanism of action. *Ann. N.Y. Acd. Sci.* **2007**, *1116*, 340–348.
(10) Bouillon, R.; Carmeliet, G.; Verlinden, L.; van Etten, E.; Verstuyf, A.; Luderer, H. F.; Lieben, L.; Mathieu, C.; Demay, M. Vitamin D and human health: lessons from vitamin D receptor null mice. *J. Steroid Biochem. Mol. Biol.* **2008**, *29*, 726–776.
(11) Vieth, R. Vitamin D toxicity, policy, and science. *J. Bone Miner. Res.* **2007**, *22*, V64–V68.
(12) Nagpal, S.; Na, S.; Rathnachalam, R. Noncalcemic actions of vitamin D receptors ligands. *Endocr. Rev.* **2005**, *26*, 662–687.
(13) Campbell, M. J.; Adorini, L. The vitamin D receptor as a therapeutic target. *Expert Opin. Ther. Targets* **2006**, *10*, 735–748.
(14) Takahashi, T.; Morikawa, K. Vitamin D receptor agonists: opportunities and challenges in drug discovery. *Curr. Top. Med. Chem.* **2006**, *6*, 1303–1316.
(15) Debb, K. K.; Trump, D. L.; Johnson, C. S. Vitamin D signalling pathways in cancer: potential for anticancer therapeutics. *Nat. Rev. Cancer* **2007**, *7*, 684–700.
(16) Glebocka, A.; Sokolowska, K.; Sicinski, R. R.; Plum, L. A.; Deluca, H. F. New 1α,25-dihydroxy-19-norvitamin D_3 compounds constrained in a single A-ring conformation: synthesis of the analogs by ring-closing methathesis route and their biological evaluation. *J. Med. Chem.* **2009**, *52*, 3496–3504.
(17) Stein, M. S.; Wark, D. L. An update on the therapeutic potential of vitamin D analogs. *Expert Opin. Invest. Drugs* **2003**, *12*, 825–840.
(18) Eelen, G.; Gysemans, C.; Verlinden, L.; Vanoirbeek, E.; DeClercq, P; Van Haver, D.; Mathieu, C.; Bouillon, R.; Verstuyf, A. Mechanism and potential of the growth-inhibitory actions of vitamin D and analogs. *Curr. Med. Chem.* **2007**, *14*, 1893–1910.
(19) Hourai, S.; Rodrigues, L. C.; Antony, P.; Reina-San Martin, B.; Ciesielski, F.; Magnier, B. C.; Schoonjans, K.; Mouriño, A.; Rochel, N.; Moras, D. Structure-based design of a superagonist ligand for the vitamin D nuclear receptors. *Chem. Biol.* **2008**, *15*, 383–392.
(20) Hourai, S.; Fujishima, T.; Kittaka, A.; Suhara, Y.; Takayama, H.; Rochel, N.; Moras, D. Probing a water channel near the A-ring of receptor-bound 1a,25-dihydroxyvitamin D_3 with selected 2 alpha-substituted analogs. *J. Med. Chem.* **2006**, *49*, 5199–5205.
(21) Konno, K.; Fujishima, T.; Maki, S.; Liu, Z.; Miura, D.; Chokki, M.; Ishizuka, S.; Yamaguchi, K.; Kan, Y.; Kurihara, M.; Miyata, N.; Smith, C.; DeLuca, H. F.; Takayama, H. Synthesis, biological evaluation, and conformational analysis of A-ring diastereomers of 2-methyl-1,25-dihydroxyvitamin D_3 and their 20-epimers: unique activity profiles depending on the stereochemistry of the A-ring and at C-20. *J. Med. Chem.* **2000**, *43*, 4247–4265.
(22) Hughes, G.; Kimura, M.; Buchwald, S. L. Catalytic enantioselective conjugate reduction of lactones and lactams. *J. Am. Chem. Soc.* **2003**, *125*, 11253–11258.
(23) Trost, B. M.; Dumas, J.; Villa, M. New strategies for the synthesis of vitamin D metabolites via Pd-catalyzed reactions. *J. Am. Chem. Soc.* **1992**, *114*, 9836–9845.
(24) For the use of carvones in the synthesis of vitamin D_3 A-ring fragments, see the following: (a) Baggiolini, E. G.; Iacobelli, J. A.; Hennessy, B. M.; Uskokovic, M. R. Stereoselective total synthesis of 1α,25-dihydroxycholecalciferol. *J. Am. Chem. Soc.* **1982**, *104*, 2945–2948. (b) Baggiolini, E. G.; Iacobelli, J. A.; Hennessy, B. M.; Batcho, A. D.; Sereno, J. F.; Uskokovic, M. R. Stereocontrolled total synthesis of 1α,25-dihydroxycholecalcifero1 and 1α,25-dihydroxyergocalciferol. *J. Org. Chem.* **1986**, *51*, 3098–3106. (c) Aurrecoechea, J. M.; Okamura, W. H. A short, enantiospecific synthesis of the 1α-hydroxyvitamin D enyne A-ring synthon. *Tetrahedron Lett.* **1987**, *28*, 4947–4950. (d) Baggiolini, E. G.; Hennessy, B. M.; Iacobelli, J. A.; Uskokovic, M. R. Stereospecific synthesis of the Lythgoe's ring a aldehyde for the preparation of 1α-hdroxylated tachysterols and

calciferols. *Tetrahedron Lett*. **1987**, *28*, 2095–2098. (e) Castedo, L.; Mascareñas, J. L.; Mouriño, A. An improved synthesis of 1α,25-dihydroxyvitamin D A synthons. *Tetrahedron Lett*. **1987**, *28*, 2099–2102. (f) Okamura, W. H.; Aurrecoechea, J. M.; Gibbs, R. A.; Norman, A. W. Synthesis and biological activity of 9,11-dehydrovitamin D_3 analogues: stereoselective preparation of 6β-vitamin D vinylallenes and a concise enynol synthesis for preparing the A-ring. *J. Org. Chem*. **1989**, *54*, 4072–4083. (g) Hatakeyama, S.; Numata, H.; Osanai, K.; Takano, S. Efficient enantiospecific synthesis of key A-ring synthons for the preparation of 1α,25-dihydroxyvitamin D_3 using a chromium-(II)-mediated reaction. *J. Org. Chem*. **1989**, *54*, 3515–3517. (h) Mascareñas, J. L; Sarandeses, L. A.; Castedo, L.; Mouriño, A. Palladium-catalysed coupling of vinyl triflates with enynes and its application to the synthesis of 1α,25-dihydroxyvitamin D_3. *Tetrahedron* **1991**, *47*, 3485–3498. (i) Maestro, M. A.; Castedo, L.; Mouriño, A. A convergent approach to the dihydrotachysterol diene system. Application to the synthesis of dihydrotachysterol$_2$ (DHT_2), 25-hydroxydihydrotachysterol$_2$ (25-OH-DHT_2), 10(R),19-dihydro-(5E)-3-epivitamin D_2 and 25-hydroxy-10(R),19-dihydro-(5E)-3-epivitamin D_2. *J. Org. Chem*. **1992**, *57*, 5208–5213. (j) Mouriño, A.; Torneiro, M.; Vitale, C.; Fernández, S.; Pérez-Sestelo, J.; Anné, S.; Gregorio, C. Efficient and verstile synthesis of A-ring precursors of 1α,25-dihydroxy-vitamin D_3 and analogues. Applications to the synthesis of Lythgoe−Roche phosphine oxide. *Tetrahedron Lett*. **1997**, *38*, 4713–4716. (k) Gómez-Reino, C.; Vitale, C.; Maestro, M.; Mouriño, A. Pd-catalyzed carbocyclizatrion-Negishi cross-coupling cascade: a novel approach to 1α,25-dihydroxyvitamin D_3 and analogues. *Org. Lett*. **2005**, *7*, 5885–5887.

(25) (a) Klein, E.; Ohloff, G. Der stereochemische verlauf der alkalischen epoxydation von α,β-ungesättigten carbonylverbindungen der cyclischen monoterpenreihe. *Tetrahedron* **1963**, *19*, 1091–1099. (b) Daniewski, A. R.; Garafolo, L. M.; Hutching, S. D.; Kabat, M. M.; Liu, W.; Okabe, M.; Radinov, R.; Yiannikouros, G. P. Efficient synthesis of the A-ring phosphine oxide building block useful for 1α,25-dihydroxyvitamin D_3 and analogues. *J. Org. Chem*. **2002**, *67*, 1580–1587.

(26) Tocchini-Valentini, G.; Rochel, N.; Wurtz, J. M.; Mitschler, A.; Moras, D. Crystal structures of the vitamin D receptor complexed to superagonist 20-epi ligands. *Proc. Natl. Acad. Sci. U.S.A*. **2001**, *98*, 5491–5496.

(27) Rochel, N.; Tocchini-Valentini, G.; Egea, P. F.; Juntunen, K.; Garnier, J. M.; Vihko, P.; Moras, D. Functional and structural characterization of the insertion region in the ligand binding domain of the vitamin D nuclear receptor. *Eur. J. Biochem*. **2001**, *268*, 971–979.

(28) Eelen, G.; Verlinden, L.; Rochel, N.; Claessens, F.; De Clercq, P.; Vandewalle, M.; Tocchini-Valentini, G.; Moras, D.; Bouillon, R.; Verstuyf, A. Superagonistic action of 14-epi-analogs of 1,25-dihydroxyvitamin D explained by vitamin D receptor−coactivator interaction. *Mol. Pharmacol*. **2005**, *67*, 1566–1573.

(29) Tocchini-Valentini, G.; Rochel, N.; Wurtz, J. M.; Moras, D. Crystal structures of the vitamin D nuclear receptor liganded with the vitamin D side chain analogs calcipotriol and seocalcitol, receptor agonists of clinical importance. Insights into a structural basis for the switching of calcipotriol to a receptor antagonist by further side chain modification. *J. Med. Chem*. **2004**, *47*, 1956–1961.

(30) Rochel, N.; Moras, D. Ligand binding domain of vitamin D receptors. *Curr. Top. Med. Chem*. **2006**, *6*, 1229–1241.

(31) Yamamoto, K.; Inaba, Y.; Yoshimoto, N.; Choi, M.; DeLuca, H. F.; Yamada, S. 22-Alkyl-20epi-1alpha,25dihydroxyvitamin D3 compounds of superagonistic activity: syntheses, biological activities and interaction with the receptor. *J. Med. Chem*. **2007**, *50*, 932–939.

(32) Suhara, Y.; Nihei, K. I.; Tanigawa, H.; Fujishima, T.; Konno, K.; Nakagawa, K.; Okano, T.; Takayama, H. Syntheses and biological evaluation of novel 2alpha-substituted 1alpha,25-dihydroxyvitamin D3 analogs. *Bioorg. Med. Chem. Lett*. **2000**, *10*, 1129–1132.

(33) Suhara, Y.; Kittaka, A.; Kishimoto, S.; Calverley, M. J.; Fujishima, T.; Saito, N.; Sugiura, T.; Waku, K.; Takayama, H. Synthesis and testing of 2alpha-modified 1alpha,25-dihydroxyvitamin D_3 analogs with a double side chain: marked cell differentiation activity. *Eur. J. Biochem*. **2000**, *12*, 3255–3258.

(34) (a) Okamura, W. H. Vitamin D Nomenclature: A Chemist's Viewpoint. In *Vitamin D: Basic Research and Its Clinical Application*; Norman, A. W., Schaefer, K., Herrath, D. V., Eds.; Walter de Gruyter: Berlin, 1979. (b) Coffey, S. *Rodd's Chemistry of Carbon Compounds. Vol II. Steroids*; Elsevier: London, 1970. (c) Definitive rules for nomenclature of steroids. *Pure Appl. Chem*. **1972**, *31*, 283−322.

(35) Otwinowski, Z.; Minor, W. Processing of X-ray data collected in oscillation mode. *Methods Enzymol*. **1997**, *276*, 307–326.

(36) Murshudov, G. N.; Vagin, A. A.; Dodson, E. J. Refinement of macromolecular structures by the maximum-likelihood method. *Acta Crystallogr*. **1997**, *D53*, 240–255.

(37) Emsley, P.; Cowtan, K. Coot: model-building tools for molecular graphics. *Acta Crystallogr*. **2004**, *D60*, 2126–2132.

(38) Laskowski, R. A.; MacArthur, M. W.; Moss, D, S.; Thornton, J. M. PROCHECK: a program to check the stereochemical quality of protein structures. *J. Appl. Crystallogr*. **1993**, *26*, 283–291.

(39) Champy, M. F.; Selloum, M.; Piard, L.; Zeitler, V.; Caradec, C.; Chambon, P; Auwerx, J. Mouse functional genomics requires standardization of mouse handling and housing conditions. *Mamm. Genome* **2004**, *15*, 768–783.